UNITED STATES DEPARTMENT OF THE INTERIOR
GEOLOGICAL SURVEY

Reconnaissance gas chemistry of the Creede, Colorado, hydrothermal system

by

Gary P. Landis[1]
and
Robert O. Rye[1]

Open-File Report 89-84

1989

[1]U.S. Geological Survey
Denver, Colorado

This report is a reformatted and greatly amplified version of a talk presented at the San Juan Volcanic Field Symposium, Rocky Mountain Geological Society of America Sectional Meeting, Boulder, Colorado, May, 1987 (Landis and Rye, 1987). Because the talk was presented as one of a series on epithermal mineralization at Creede, some references in this report to other talks in the series or to district geological features may be unfamiliar to the reader. For background, the reader is referred to Hayba et al. (1985), Barton et al. (1977) and to Open-File reports of the symposium talks (Bethke, 1988; Plumlee et al., 1988; Rye et al. 1988) as well as to abstracts of the other talks (Foley et al., 1987; Hayba, 1987; Barton, 1987).

ABSTRACT

The gas chemistry (H_2O, CO_2, H_2S, SO_2, Ar, N_2, CH_4, and various organic species) of the Creede hydrothermal fluids was determined from inclusion fluids in samples representative of the time space features of the hydrothermal system as indicated by previous stable isotope studies of the fluids and host minerals. In addition, gas chemistry studies were made on samples that have been the subject of detailed fluid inclusion temperature and salinity studies. The gas chemistry of the Creede hydrothermal system was highly variable in time and space. The gas compositions are significant indicators of the sources and evolution of fluids in the veins and at depth. Each major stage of mineralization is characterized by a specific gas chemistry which may have been modified locally by mixing and/or boiling. The gas compositions of fluids derived from the highlands in the northern part of the district are distinct from fluids derived from the sediments in the moat of the Creede caldera in the south. Fluids from all paragenetic stages, including those from the high-T (up to 310°C) and high fO_2 (hematite stable) main stages, contain a complex (and as yet poorly-characterized) mixture of alkanes, alkenes, and aromatic hydrocarbons. These hydrocarbons must have been derived from progressive thermal degradation or pyrolysis of moat sediment organic matter in the southern part of the district and from a hidden source of saturated hydrocarbons in the northern part of the district. The presence of significant quantities of SO_2 in some of the fluids suggests the formation of metastable thiosulfate during mixing of the hydrothermal fluids with low pH fluids in the overlying groundwater. The persistence of the organic species and disequilibrium gas compositions in the fluids both indicate lack of attainment of complete chemical equilibrium in the system consistent with interpretations based on the chemical and sulfur isotope composition of ore minerals.

To obtain these gas chemistry data, samples were heated in a vacuum furnace with a programmed temperature rise. Computerized, real-time multiple ion monitoring on the gases released was performed by quadrupole mass spectrometer. Thermal gas release profiles define discrete populations of fluid inclusions that can be distinguished from adsorbed/desorbed gas release, the thermal decomposition of host minerals and occult solid inclusions, and "matrix gas" released from submicron-sized fluid inclusions, domain boundaries, micro-structures, crystal defects, and gas dissolved in the crystal. Possible gas reactions and pyrolysis during decrepitation are evident from product and reactant profiles. Superimposed upon the thermal profiles are sharply-defined spikes that represent sudden release of gas from single or multiple fluid inclusions. Quantitative analysis of these "bursts" permits detailed study of ore fluid chemistry at the level of individual fluid inclusions. Gas partial pressures were determined from the mass spectrometer data with gas-specific correction factors that include the ion sensitivity and fragmentation, kinetic rates of adsorption/desorption on vacuum surfaces and differential vacuum pumping.

INTRODUCTION

Gases exist in hydrothermal fluids both as solutes and as a separate phase. They occur in ore and gangue minerals both in substitution in crystal structures and trapped in fluid

inclusions. They also are absorbed on crystal surfaces. The most direct method of determining their abundances in hydrothermal fluids is by analyses of inclusion fluids. Gas abundance data help to indicate sources, prevailing fluid/rock processes, and environmental (physical-chemical) conditions of hydrothermal systems. As such, gas data provide overlapping and complimentary information to that obtained from stable isotope and fluid inclusion temperature and salinity studies and from the interpretation of mineral assemblages. The purpose of this presentation is twofold: (1) to clarify sources and processes in the Creede system; (2) to demonstrate that gas chemistry data, when combined with well documented fluid inclusion and stable isotope data, provide an exceptionally powerful tool to study processes in any hydrothermal system.

This is a reconnaissance study of the Creede hydrothermal system. Subsequent studies will provide much closer paragenetic constraints and will be more closely tied to individual fluid inclusion type, paragenesis, temperature, salinity, and stable isotope measurements. However, by taking advantage of the exceptional geochemical framework developed in various studies on Creede we have been able to choose samples to characterize the basic gas geochemistry of the hydrothermal system. In this study we have 1) obtained quantitative gas composition data from individual fluid inclusions in samples previously characterized by petrographic, micro-thermometric, and related stable isotope studies, 2) demonstrated that each of the several major fluids in the Creede system has distinctive gas chemistry, 3) demonstrated that the mixing of these fluids and their chemical evolution by fluid-rock reactions, and phase separation and condensation can be recognized and studied by gas chemistry data, 4) documented aqueous sulfur species metastability and probable thiosulfate formation in the hydrothermal system as indicated by disequilibrium amounts of sulfur dioxide gas that correlate with the hydrologic structure of the hydrothermal system, and 5) traced the origin and evolution of light chain and aromatic hydrocarbons in the system.

ANALYTICAL PRINCIPLES AND METHODS

FIGURE 1: *Schematic diagram of a quadrupole mass spectrometer*

Basically, the quadrupole mass spectrometer (QMS) is comprised of four rods, or poles, a gas ionization source region at one end of the rods, and a ion detection system (secondary electron multiplier) at the other end. Quadrupole mass spectrometers do not require a massive magnet to generate magnetic fluxes, but rather use simple rf waveforms on the rods to create mass dispersion and spectral analysis. This QMS system is preferable in gas analyses because it is capable of scans as fast as 100 microseconds/atomic mass unit (AMU) and is extremely sensitive with lower limit for routine analyses of individual gas species in the 10 ppm range (10 ppb range with special tuning) and AMU detection limits as low as 8×10^{-15} mbar (2X background). An extremely stable instrument capable of maintaining 1/64th AMU mass resolution over a 24 hour period, it has a linear mass scale output of mass resolution adequate for gas speciation and quantitative analysis (unit resolution to approximately 200 AMU).

FIGURE 2: *Schematic Block Diagram of Fluid Inclusion Gas Analysis System*

The diagram illustrates the essential components of the fluid inclusion gas analysis system. The main QMS is pumped by a turbomolecular pump and backup ion pump with a safety interlock gate valve. A secondary QMS is positioned with an intervening liquid N_2 cryrotrap to simultaneously monitor non-condensable gas species. Leak valves on the inlet permit precise control on sample (or reference gas) conductance to the QMS ion source. Furnaces, cryogenic traps for gas separation, vacuum gauges, and auxiliary turbomolecular vacuum pumping enable bulk and thermal profile gas analysis. The dual inlet design enables both sample gas mixtures and prepared reference gases to be compared.

The system has two thermal profile furnaces (affectionately called "hotdog" furnaces) with a small quartz capsule containing fluid inclusion material. It is important to

understand that gas from the host mineral is generated by heating the sample at a uniform rate of about 10°C/min to cause decrepitation of the contained fluid inclusions. All sample gases are pumped through the ion source and continuously monitored by the computer-driven QMS. The gases from individual fluid inclusions are detected using high speed real-time data collection. Fluid inclusion gases are distinguished from gases due to the rise in background with heating, from thermal decomposition of host minerals, and from pyrolysis of generated gases. Although heating opens all types of inclusions during the thermal ramps secondary and primary inclusion populations can often be differentiated by their bursting temperatures and compositions.

FIGURE 3: *Thermal Profile of Gas Release -- OH Vein Sphalerite -- Monitoring H_2S*

The actual graphics screen display from the computer is shown in this figure, in which, the variation in intensity of the mass 34 ion (H_2S gas primary peak) and mass 17 ion (OH peak for water) is plotted through temperature during the thermal ramp of a sample of sphalerite. This sample was prepared from polished plates which contained four fluid inclusions that had been measured previously for filling and freezing temperatures. Since the temperature of the furnace is ramped at constant rate, the abscissa can be time, temperature, or successive equally spaced measurement cycle data points. The rapid increase in intensity represents the release of fluid inclusion-contained hydrogen sulfide gas which the QMS "sees" as mass 34. In this example the four fluid inclusions were opened, each with its own "burst" release profile spike. In general, a burst event can represent either the opening of a single fluid inclusion or of a very small number of neighboring fluid inclusions opened by the same decrepitation crack. Note that the intensity is plotted in log units, and that an individual fluid inclusion burst typically takes 10-100 milliseconds to reach maximum peak intensity before decaying due to dynamic pumping. Quantitative information comes from attributing the net increase in intensity of the peak (above the immediately preceding background intensity) to the gas released from the "burst event". Peak intensities of interest are tracked in real-time and the data stored on disk. Typically 8-10 MBytes of data are acquired during an analysis. Graphic manipulation to produce plots like those in this figure and matrix calculations to obtain quantitative data are completed later.

Because H_2O is a polar molecule and behaves 'sticky' in a vacuum system, its pumpdown recovery after each fluid inclusion burst is spread out over a longer time period than that for hydrogen sulfide. The pumpdown profile illustrates the theoretically predicted log-linear recovery immediately after a burst event. Eventually kinetically controlled surface desorption gas release modifies the linear portion of the curve. As H_2O is the gas most prone to adsorption in a vacuum system, it exhibits the slowest pumpdown recovery. As it normally is the predominant gas, H_2O can cause problems of detection of other gases and sometimes must be removed cryogenically during the analysis. A net intensity vector (height of peak above the local background) for all peaks monitored by the QMS is the final analytical result. The kinetics of burst pumpdown recovery introduces an uncertainty in determining the area under the peak, therefore maximum peak intensity data are used instead of integrated peak area. Very rapid data collection is necessary in order to clearly define the maximum of the burst peak.

FIGURE 4: *Matrix Calculation*

The data are reduced to quantitative gas analyses by means of matrix algebra. The analytical result is a net intensity vector representing the intensity for each mass in the spectrum from the gas mixture released from the decrepitated fluid inclusion. The QMS is calibrated with reference gases to previously establish the ion fragmentation patterns of the gases of interest and the ionization efficiency of each gas relative to nitrogen. These data form the calibration matrix and sensitivity vector multiplier. The partial pressures of each gas in the mixture are determined by solving this matrix in a general form by standard least squares methods. The precision of the analysis is about 3-5 percent of the amount

reported, with samples as small as about 10 ppm of the total gas. The mean diameter of the smallest fluid inclusion for which gas content can be analyzed by the present instrumental configuration while maintaining this precision is about 10 microns. Below this size, vacuum conductance of gases approach kinetics of sorption.

The equations show the general solution to the matrix calculation. |A| is the general matrix of **m** peaks by **n** gas species and contains gas ion fragmentation and sensitivity data from instrumental calibration (combined calibration matrix and sensitivity vector). $\mathbf{A^T}$ is the transpose of |A|. **Q** is the inner (minor) product of |A| and $\mathbf{Q^{-1}}$ the inverse of **Q**. |P| is a **n**-vector of gas species (vector of gas partial pressures) and |I| the **m**-vector of peak intensities determined from the burst analysis (intensity vector). The solution for |P| is obtained by a least squares and iterative numerical process. The gas species that comprise |P| are chosen by the operator based upon the intensities in the AMU vector |I|, and upon general knowledge and geochemical reasonableness for suspected gas species to be present. If the most abundant mass fragment for a given gas specie is not detected, then it is not present in the fluid inclusion gas mixture. Otherwise, the researcher is forced to solve the matrix problem a number of times, searching for a geochemically reasonable set of gases that numerically minimizes the least squares residuals to the solution. To help judge the reasonableness of the solution derived from the selected gas species, an average absolute **residual** and a residual factor for each AMU intensity are computed using the |P| solution. An average absolute **residual** is the sum of absolute residuals on each AMU divided by the number of AMU's. An individual AMU residual is the difference between the measured intensity at a given mass and that intensity computed by summing the percentage contribution from each gas to the intensity, weighted by the partial pressures (mole fractions) calculated for each gas. The accepted solution is one that best accounts for the intensity at each AMU with a minimum residual, by selection of geochemically reasonable gases. The average absolute **residual** for results are tabulated in the Appendicies 2-6 data tables.

Another useful number, first calculated only after many analyses had been completed, is **contrast. Contrast** is reported as the sum of all "burst" intensities, divided by the sum of all immediately preceding background intensities. This parameter is reported in the Appendicies only for more recently generated data sets. It is a measure of the overall intensity difference between fluid inclusion gas and the "local" background immediately prior to the "burst". In other words, it is an approximate indication of the relative size of an inclusion, and provides a means to compare the amount of gas released by a series of inclusion "bursts".

The partial pressures of each gas in the mixture calculated by this method can be viewed as mole fraction of the gas. The absolute quantity of each gas is easily determined by assuming ideal gas behavior and calibrating the ionization source (amps/mbar). However, in routine operation the relative measurements expressed as partial pressures or mole fractions are sufficient.

APPLICATIONS TO CREEDE

All of the samples for inclusion gas analyses were selected on the basis of stable isotope (Rye et al, 1988) and/or fluid inclusion (Hayba, 1985) information on the samples. In most cases analyses were made on chips that were as near as possible to the site of the original stable isotope analyses, or were the actual inclusions on which fluid inclusion measurements were made. A summary of isotope and fluid inclusion data on the samples are given in Appendix 1. The complete gas compositions of all samples are listed in the Appendices 2-6. No attempt is made to distinguish primary, secondary, or necked inclusions although these can often be recognized from their burst temperatures and fluid compositions. The data are plotted as a series of ternary gas composition diagrams which show the relative gas compositions of the fluids as normalized mole percents. H_2O is plotted as 1/100 of its mole percent in order to better visualize the grouping of data. Total organics are C_2 through C_6, excluding CH_4. Total sulfur is H_2S+SO_2. These ternaries

are grouped in figures to show: 1) the different ternary gas compositions shown by groups of samples previously studied for stable isotope compositions (ie., δD_{H2O}-$\delta^{18}O_{H2O}$ of inclusion fluids, $\delta^{13}C$-$\delta^{18}O$ of carbonates, $\delta^{34}S$-$\delta^{18}O$ of barites 2) the gas composition of fluids from the Northern exploration area (NEA) versus those from the southern part of the district 3) gas chemistry of a single sample of quartz from the OH vein containing primary, pseudosecondary, and secondary inclusions and 4) various ternary gas compositions of all samples from the district. In the following discussions, qualitative expressions about compositions on ternary diagrams refer to variations with respect to end member components. Thus, a sample refered to as sulfur rich need not have high absolute total sulfur.

FIGURE 5: *Map of the Creede mining district (modified from Steven and Eaton, 1975)*
This map shows the location of the major veins in the NEA and the southern district which is bounded on the south by the moat sediments of the Creede caldera. Most samples in this study were from the Equity, Bulldog Mountain, OH, and Amethyst veins

FIGURE 6: *N-S Diagrammatic Longitudinal Section of the Creede Hydrothermal System*
This is a N-S longitudinal section through the district showing a schematic model of the main stage Creede hydrology as presented by Bethke (1988) and Rye et al. (1988). These references should be consulted for meaning of rock unit symbols. The section shows the spatial relations of various fluids analyzed for gas chemistry in this study. The shaded area that represents the upwelling plume, of high temperature hydrothermal fluids, is defined by the 200°C isotherm. From the plume origins at depth the flow path is up and then diverted south, eventually reaching the moat sediments of the Creede Formation. This southerly distortion of the plume is caused by the incursion of shallow overlying groundwater coming off the continental divide to the north. Several fluid components are recognized and marked by large block letters. They include: [N] *Northern Recharge* waters, possibly from reservoirs in the San Luis Peak caldera fill or La Garita caldera, recharged into the northern part of the hydrothermal system; [S] *Southern Recharge* waters chemically and isotopically evolved in the moat sediments of the Creede caldera and recharged at various levels ([S], deep; [S'], shallow) into the convective system; [D] *Deep* waters, either of magmatic origin or of very deep, but undefined origin, chemically equilibrated at high temperatures with igneous rocks; [G] *Shallow Ground* water from northern recharge off the continental divide and overlying the upwelling plume; [MN] *Mixed Northern* waters, mixed or interfacing Northern Recharge [N] and Southern Recharge [S] waters in the deeper parts of the upwelling plume; [MS] *Mixed Southern* waters, mixtures of water of the upwelling plume with pore fluids in the moat sediments; and [MO] *Mixed Overlying* waters, mixtures of water of the upwelling plume with overlying ground waters [G]. Some of these fluid components have characteristic gas chemistries as will be summarized after presentation of data on fluids for various mineral groups in the district. Much of the mineralization occurred in the zone of mixing between the upwelling plume and the overlying ground waters [G] and moat sediment pore fluids [S'].

Gas chemistry of the barite fluids

FIGURE 7: *$\delta^{34}S$ and $\delta^{18}O$ of barites from the Creede district*
Rye et al. (1988) interpreted the $\delta^{34}S$ and $\delta^{18}O$ data on barite to indicate that *sulfate* in the Creede system was derived from three sources with the "end member compositions" shown in Figure 7. These sources were a) sulfate from interstitial fluids of the moat sediments without significant reduction, b) sulfate from interstitial fluids of the moat sediments which underwent partial reduction during recharge into the intermediate levels of the hydrothermal system and/or along the interface between the pore fluids and spent hydrothermal fluids, and c) deep hydrothermal sulfate generated by equilibrium oxidation of H_2S from magmatic or volcanics sources. (There appears to have been *relatively* little

sulfate from shallow oxidation of H_2S at Creede.) Four representative barite samples whose isotopic compositions fall near the end member values, and are presumed to have been precipitated from fluids which contained "end member" sulfate compositions were selected for fluid inclusion gas analysis and are indicated by sample numbers in the figure.

FIGURE 8: *Fluid inclusion gas chemistry in representative barites*

This figure shows the gas compositions of 76 fluid inclusion from the four barites. Although there is a significant amount of overlap the NEA barite fluids with deep sulfate tend to have higher total sulfur (Figure 8 A), higher total organics (Figure 8 B), higher H_2S relative to SO_2 (Figure 8 C) and higher CH_4 (Figure 8 D) than the barite fluids with sulfate from moat sources. As will be shown later, the organics of the NEA fluids also have a greater proportion of aromatic to light chain hydrocarbons (Figure 19). The relatively low H_2S content of the fluids with moat sediment-derived sulfate is not surprising because H_2S in the moat sediment pore fluids was probably formed by earlier bacterial reduction of sulfate and precipitated as pyrite. Barite at the southern end of the district probably precipitated in response to mixing of these sulfate rich fluid with sulfate rich hydrothermal fluids (MS environment in Figure 6). We can not measure the sulfate content of the barite fluids but unexpectedly, the fluids in barites with moat sediment-derived sulfate are relatively high in SO_2. The QMS method can detect SO_2 to approximately 10^{-4} molal, but the analyses indicate 10^{-1} to 10^{-3} molal SO_2.

SO_2 in fluid inclusions

FIGURE 9: *Temperature-Molality Plot for Aqueous SO_2*

The solubility (log molality) of sulfur dioxide gas in fluids buffered by the assemblage pyrite-chlorite-hematite-Kspar-Kmica-quartz in the Creede hydrothermal system can be predicted from this temperature-molality plot. Also shown are the temperature and salinity fields of fluids in various vein systems from north to south in the district. The aqueous sulfur dioxide predicted from the calculated fluids of Creede indicate $< 10^{-7}$ molal to as little as 10^{-11} molal at equilibrium. The measured fluid compositions contain many orders of magnitude more SO_2. This gas composition must be from the fluids preserved in the inclusions. This SO_2 cannot be due to pyrolysis or redox reactions, as all reactants and products are monitored during the analysis. Nor can it be derived from aqueous sulfate during heating while decrepitating the inclusions as H_2S and SO_2 do not co-vary during the profile release. Most likely, the SO_2 in the fluids is an analytical decomposition product of some other species during heating and decrepitation of inclusion in the vacuum system QMS. We suggest that the SO_2 is produced by the decomposition of intermediate and metastable sulfur species (thiosulfates, sulfite, or other polysulfides) that were ultimately formed by of oxidation of H_2S during mixing of the hydrothermal fluids with overlying low pH groundwater.

FIGURE 10: *Thermal profile for H_2O, SO_2 and H_2S for high and low temperature primary fluid inclusions in sphalerite from the NJP-X locality in the OH vein*

The computer graphics display thermal profiles for H_2O (AMU = 17) and SO_2 (AMU = 64), and H_2S (AMU = 34) in inclusions in low (<220°C) (Q0233) and high (~285°C) (Q0234) temperature sphalerite from the NJP-X locality in the OH vein. AMU 17 is used instead of 18 because of the large size of the inclusions which release so much water they cause the 18 peak to go off scale. The high temperature sample is the same as the one in Figure 4 that shows four discrete burst spikes for individual inclusions in a sample of sphalerite. The high temperature inclusion fluids have salinities of ~12 equivalent wt.% NaCl. These fluids, which were largely from the upwelling plume and are the least mixed with overlying fluids, contain both H_2S and SO_2. As mentioned for the previous figure the SO_2 is probably related to the breakdown of thiosulfate in the fluids during decrepitation analysis of the fluid inclusions. The low temperature inclusion fluids have salinities of 7±1 equivalent wt. % NaCl. These fluids are more mixed with overlying fluids than the higher

temperature fluids and have no SO_2. These inclusion presumeably have no thiosulfate. The stability of thiosulfate is dependant on pH, fO_2, and temperature. At the onset of mixing in the higher termperature and higher pH fluids, thiosulfate probably is more abundant than at the lower temperature and lower pH (and probably higher fO_2) fluids that are more extensively mixed with the overlying groundwater. In the more mixed fluids the thiosulfate is probably completely oxidized to aqueous sulfate.

Gas chemistry of NEA fluids

FIGURE 11: *NEA fluid inclusion gas chemical compositions*

This figure portrays various ternary gas compositions of 35 fluid inclusions from two samples of quartz and one sample each of sphalerite, fluorite, and adularia from the NEA. Stable isotope data (Rye et al., 1988) indicate that fluorite, adularia and quartz were probably formed from fluids that contained a substantial component of isotopically light, northern recharge waters, whereas sphalerite formed from isotopically heavier fluids with origins to the south. The degree to which these northern and southern recharge fluids actually mixed in the plume of the system has not been determined. The southern recharge fluids traveled nearly 10 kilometers north under the district bringing components from the Creede moat sediments. Fluids from the north and south have different stable isotope compositions (Rye et al., 1988) and we would expect them also to have dramatically different gas chemistries. We suspect that the NEA overlies the heat source which drove the hydrothermal system. In support of this the highest HF contents are observed in fluid inclusion gases in samples from the NEA (Appendix 3).

In Figure 11 A the fluids of northern and southern derivation are not distinguished on the basis of total sulfur relative to CO_2. This observation is consistent with the uniform sulfur isotope composition of sulfides in the district and probably reflects the fact that sulfur in the ore system was dominated by a deep sulfur source in the roots of the upwelling plume. Notice that most of the fluids in quartz plot near the CO_2 apex. In the absence of petrographic evidence regarding the nature (boilers, necked, primary, secondary, or pseudosecondary) of these high CO_2 inclusions interpretation is not possible. If the inclusions are primary the data imply that the deep northern recharge fluids had high CO_2 during quartz deposition.

In Figure 11 B northern-derived fluids in quartz and fluorite contain abundant total organics relative to H_2O. Northern-derived waters also are characterized by greater amounts of nitrogen, including the presence of ammonia detected in a few inclusions (Appendix 3). The sphalerite fluids contain dominantly CH_4, and lack the more complex organic gases seen in fluids trapped in veins closer to the Creede moat sediments in the southern part of the district. We interpret this organic speciation in the sphalerite fluids as evidence for thermal pyrolysis of organic molecules during the northward passage of the fluids under the district to the NEA. Organics of northern derived waters have their origins in other sedimentary traps, possibly San Luis Peak moat sediments. The reason these northern-derived organics survived thermal pyrolysis while those that reached the NEA from the south did not, may be related to a much shorter residence time in the high temperature part of the hydrothermal system. Alternatively, the organics from the north may have entered the system at a low temperature shallow level.

Figure 11 D further emphasizes the distinction in organic gas content between fluids of northern and southern derivation. Unlike the fluids in fluorite, adularia, and quartz, the sphalerite fluids contain no significant total organics but are relatively rich in total sulfur and CH_4. The NEA sphalerite fluids have lost all of their original organics in the 10 kilometer northerly traverse from Creede moat sediments, under the plume, and into the NEA. The CH_4 produced by organic maturation during travel of the fluids northward under the district was probably very stable and very mobile in the Creede system.

Gas chemistry of the main and late stage fluids

FIGURE 12: *δD_{H2O}-$\delta^{18}O_{H2O}$ of the Main and Late Stage Inclusion Fluids*

The hydrogen and oxygen isotopic composition of the Creede hydrothermal fluids for early sphalerite in the NEA and main and late stage minerals in the southern district was determined by direct analyses of inclusion fluids (Rye et al., 1988). These data indicate that most fluid compositions were mixtures of two fluids. One of these was a southern recharged saline fluid with a δD of about -50‰ that was dominant during main-stage sphalerite, galena and fluorite mineralization in the southern district. The other was a dilute, northern recharged unexchanged meteoric water with a δD of about -110‰ with which the hydrothermal brines interfaced or mixed during main-stage mineralization in the southern district. The meteoric water component appears to have predominated during late-stage pyrite mineralization. There is also a suggestion of a third fluid that appears as a ^{18}O shifted northern recharged meteoric water component in some of the southern district sphalerites. Numbers in the figure indicate samples representative of the major ore forming and late stage fluids in the Creede system that were analyzed for fluid inclusion gas chemistry.

FIGURE 13: *Gas chemistry of samples used to determine the δD_{H2O}-$\delta^{18}O_{H2O}$ of the Creede fluids*

The data shown on these ternary composition diagrams consists of 100 individual fluid inclusions from chips left over after the samples were crushed and their inclusion fluids extracted and analyzed for hydrogen and oxygen isotopic compositions. It is obvious that the gas chemistry of the system varied considerably in time and space. The gas chemistry of individual samples may reflect the integrated effect of different source inputs, boiling and/or mixing processes, sulfur and organic specie disequilibrium in the system, and degree of degradation of organic matter. Some of the processes which may be illustrated in these ternaries are:

(A) *Degassing/condensation and mixing of fluids.* Figure 13 A shows a theoretical mixing line between water and the carbon dioxide - total sulfur binary. Much of the data for main stage fluids cluster around this line. We know from isotope and chemical modeling studies of Creede that mixing was the major sphalerite precipitation mechanism (Rye et al.,1988; Plumlee et al., 1989). The data for some of the fluids *could* reflect mixing. Also shown is a *schematic* boiling trajectory. During boiling residual gas compositions should 'move' away from the CO_2 apex curving upwards to H_2O reflecting the relative solubilities of CO_2 versus either H_2S+SO_2 as gases are lost during boiling relative to their Henry's Law constants. A family of residual gas composition curves could be drawn similar to the one in the figure depending on the starting gas compositions. The curved pattern produced by some of the most sulfur rich stage B-D sphalerite fluids for several localities *could* be interpreted to fall on boiling trajectories. Boiling is hard to document from fluid inclusion evidence and it is not a major precipitation mechanism at Creede (Plumlee et al., 1988). However, some degassing of hydrothermal fluids at Creede is indicated by the presence of the clay cap on the veins and future studies need to document this from the gas chemistry of fluid inclusions.

(B) *Source of fluids.* Note the progression in fluid compositions from the water-CO_2 binary towards total organics with samples from NEA to southern district and from stage C to stage B-D in Figure 13 B. The fluids of ore depositing stage B-D are the most enriched in organics and, given the isotope constraints, the organics in the southern part of the district were derived in large measure from the south. The late stage E fluids that are enriched in CO_2 probably represent collapse of the gas charged overlying waters into deeper portions of the hydrothermal system (Plumlee and Rye, 1989). It is interesting that the stage B barite fluids have lower total organics that stage B sphalerite. As indicated by the isotope data on the barite fluids many of the barite fluid inclusions were probably flushed by overlying waters during the collapse of the hydrothermal system.

(C) *Metastable sulfur species.* In Figure 13 C ore depositing fluids for stages B-D sphalerite and stage C fluorite are enriched in H_2S relative to other fluids. In this ternary, boiling would create a trajectory down and to the right, eg. from CO_2 to the H_2S-SO_2 binary, with a curved path to SO_2. The presence of SO_2, as previously discussed, reflects the presence of metastable sulfur species in the fluids. Stage E fluids which represent cooler, oxygenated fluids collapsing in on the system, are most enriched in SO_2. Again, it is important to recognize that with regards to sulfur, the Creede hydrothermal system was grossly out of equilibrium (Barton et al., 1977; Rye et al., 1988).

(D) *Degrees of degradation of organic matter.* In Figure 13 D The NEA sphalerite and OH vein stage B-D sphalerite and stage C fluorite fluids contain high CH_4 relative to total organics. This CH_4 probably was derived from the degradation of organic matter during passage of fluids from south to north underneath the district. The presence of these complex hydrocarbons in the southern district fluids has an important implications for the hydrology of the Creede system. This implies that in contrast to the NEA sphalerite fluids, most of the B-D sphalerite fluids in the southern district returned to the shallow level vein system without traveling all of the way to the NEA .

Gas chemistry of the carbonate fluids

FIGURE 14: *$\delta^{13}C$ and $\delta^{18}O$ of Creede carbonates*

This figure summarizes the carbon and oxygen isotope data on the vein pre-ore wallrock calcites and vein rhodochrosites from the Bulldog Mountain veins (BMV) and C stage siderites from the OH vein in the southern district and rhodochrosite and calcite from the NEA. In the Southern district the wallrock calcite is the earliest recognized hydrothermal mineral while veinlet calcite is the latest mineral in the NEA. An important feature of the data is that except for the BMV wallrock calcite and the NEA calcite each generation of carbonates have unique stable isotope systematics. The carbon and oxygen isotope values of BMV wall rock calcites, BMV vein rhodochrosite and NEA vein calcites show a reasonably good positive correlation The carbon and oxygen values for the C stage siderites show a negative correlation. The range of data for each generation of carbonates is too large to be due solely to temperature variations in the hydrothermal fluid. These ranges must involve the mixing of water of different $\delta^{18}O$ as well as mixing of carbon of different $\delta^{13}C$ in the system. It is also possible that some variation resulted from a oscillation between a CO_2 and HCO_3^- dominant system. The possible carbon sources include CO_2 from the moat, CO_2 from a deep seated source or volcanic rocks, organic matter in the moat sediments and the NEA area and other shallow sources such as may have been available to the shallow ground water. Detailed interpretation in terms of fluid history is not possible until the paragenesis of the NEA mineralization and temperatures of carbonate deposition are better constrained. We hope that the gas data will help sort out the source of carbon for these different carbonates. The sample numbers indicate the samples whose inclusions were analyzed for gas chemistry.

FIGURE 15: *Gas composition of inclusion fluids from southern district carbonates*

Each generation of carbonate fluids has distinct gas chemistry. Of particular interest is the low total sulfur relative to CO_2 in the rhodochrosite fluids (Figure 15 A) the high total organics relative to CO_2 of the wall rock fluids (Figure 15 B), the high H_2S relative to SO_2 in the wall rock fluids (Figure 15 C), and the high SO_2 relative to H_2S and the high total sulfur relative to total organics in the C stage siderite fluids (Figure 15 C and D). The low sulfur content of the rhodochrosite fluids is consistent with the absence of cogenetic sulfides and the relatively high CO_2 contents are consistent with effervescence of CO_2 as a precipitation mechanism. The C stage siderite fluids have much lower total S than the earlier C stage fluorite fluids (Figure 13A). The relatively high SO_2 content of the siderite fluids may suggest that the sparse C stage siderites formed near the interface of the hydrothermal with overlying oxidizing fluids possibly during a momentary collapse in the hydrothermal system.

FIGURE 16: *Gas composition of inclusion fluids from NEA carbonates*

The gas compositions of the inclusion fluids in NEA rhodochrosites and late calcite are generally similar to those of the fluids in the southern district rhodochrosites and the wallrock calcites, respectively. Both NEA and southern district carbonate fluids may have high CH_4 relative to light chain hydrocarbons. This CH_4 probably derived from the degradation of organic matter consistent with an extensive source of saturated hydrocarbons in both the northern and southern part of the district. The organic matter in the southern fluids was probably continuously degraded to CH_4 during passage northward beneath the district.

Gas chemistry of primary and secondary quartz fluids

FIGURE 17: *Gas chemistry of inclusion fluids in quartz from the PMB-BY locality in the OH vein*

The fluid inclusions in quartz in from the PMB-BY locality have been the subject of detailed study by Foley et al (1982; in press). This quartz contains both primary and pseudosecondary inclusions which have different salinities and δD_{H2O} values. The primary fluids are isotopically similar to the main stage ore fluids, while the pseudosecondary fluids compositions are more like those of meteoric water. Foley et al. (in press) interpreted this phenomena to indicate the episodic incursion of overlying ground water into the ore zone during the time of mineralization. The sudden incursion of cooler water caused thermal cracking in the quartz and trapping of pseudosecondary inclusions. We anticipated that the pseudosecondary fluids from the overlying fluids would be high in CO_2 and SO_2 while the primaries would be typical of those previously observed in main stage sphalerites. This figure shows the gas data of a sample containing predominantly primary inclusions but probably also some secondaries. Unfortunately, a sample containing predominantly pseudosecondary inclusions was lost during analyses. When the plots in this figure are compared with those in Figure 13 for fluids in main stage sphalerite most of the gas compositions are similar, which is to be expected since the quartz and sphalerite formed from similar fluids. The most notable differences in gas compositions are the high CO_2 and SO_2 in some of the PMB BY fluids (Figure 17 A,B,C) and the high total sulfur relative to total organics in the fluids (Figure 17 D). These compositions are similar to those observed for the fluids in late stage minerals (See Figure 13) which formed during the collapse of the hydrothermal system and are reasonable for overlying fluids in the Creede system consistent with the interpretation of Foley et al. (in press) for the formation of the pseudosecondary fluid inclusion in this sample.

Summary gas compositions of the Creede fluids

FIGURE 18: *CH_4 -light chain -aromatic hydrocabon-gas compositions throughout the district*

When hydrocarbons undergo thermal maturity aromatic (saturated) hydrocarbons break down through a series of light chain hydrocarbons (LCHC) to CH_4. This could be the origin of the high CH_4 in some samples in Figure 18. As previously mentioned (Figure 11) CH_4 is the only hydrocarbon detected in the NEA sphalerite fluids which isotope data indicate were derived from the southern moat (Figure 18 A and C). Presumably the original organic fraction was thermally decomposed during northward passage under the district from the moat sediments. All of the other NEA fluids which isotope data indicate were derived from northern sources have significant organic contents and the highest aromatic to LCHC in the district. This gas chemistry implies a northern as well as southern source of organic matter (Figure 18 C) although some of the variations in organic gas chemistry could result from boiling as indicated by the schematic trends for residual fluids in Figure 18 D. There are aromatic hydrocarbons in most fluids from the southernmost part of the district and some of the stage B-D sphalerite fluids in the southern district have high CH_4 and aromatics relative to LCHC.

FIGURE 19: *CO_2-total sulfur-total organic compositions throughout the district*

There is a tremendous variation in the CO_2-total sulfur-total organic compositions of the Creede fluids. The NEA sphalerite and late stage pyrite fluids have high total sulfur relative to total organics (Figure 19 A and C). All of the carbonate fluids in the district except C stage siderites (symbols are buried near CO_2 apex in Figure 19 D) have high total organic relative to total sulfur (Figure 19 D). There was very little sulfur in the fluids during carbonate deposition. Most carbonates at Creede probably precipitated from degassing of CO_2 (Plumlee et al., 1989). The trend of the gas compositions for the carbonate fluids data does not fit the schematic curves for degassed residual fluids in Figure 19 D but looks more like a mixing trend. We suspect the composition trend reflects the way batches of residual fluids and condensed gases mixed during carbonate deposition. The large organic relative to CO_2 in the carbonate fluids suggest that some of the variation in $\delta^{13}C$ values of the carbonates (Figure 14) was related to the breakdown of organic matter. Both the late stage pyrite (Figure 19 A) and the C stage siderite (Figure 19 B) fluids have very little organic matter. Plumlee and Rye (1988) have interpreted that the late stage pyrites formed during the collapse of the overlying low pH waters in to the veins in the waning stages of the hydrothermal system. We suspect that the sparse C stage carbonates formed during a momentary collapse in the system following the deposition of fluorite which was likely related to a pulse of fluid from a magmatic source. The gas compositions for most of the ore fluids that fall in the center of the ternaries probably reflect the combined effect of the degassing of the hydrothermal fluids and their mixing with overlying fluids.

FIGURE 20: *CO_2-H_2S-SO_2 gas compositions throughout the district*

The gas compositions in this figure emphasize the time-space variations in the CO_2-H_2S-SO_2 chemistry of the fluids. Shallow fluids that appear in barite fluid inclusions (Figure 20 B) generally are CO_2 and SO_2 dominant, consistent with flushing of the inclusions by overlying groundwater after mineralization (Rye et al., 1988). Stage B-D ore stage fluids have H_2S as dominant sulfur specie (Figure 20 A). The E stage (Figure 20A) and C stage (Figure 20 D; symbols are hidden near CO_2 apex) siderite fluids are SO_2 dominant relative to H_2S, consistent with precipitation from low pH, gas charged overlying groundwaters that entered the veins during the collapse of the hydrothermal system (Figure 20 B). Carbonate fluids generally are CO_2 dominant (Figure 20 D). It is interesting to note that early wall rock calcite fluids are enriched in H_2S relative to SO_2 which is consistent with the possibility that H_2S was leached from the volcanics by the earliest fluids.

FIGURE 21: *Summary of gas chemistry of the various fluid components in the Creede system*

By integrating all of the gas, fluid inclusion and stable isotope data on fluids in various minerals in time and space a general summary can be constructed for the gas chemistry of the major fluid components in the Creede system as shown in Figure 6. This summary is highly generalized and verification and refinement is the object of detailed studies currently in progress.

CONCLUSIONS

Although reconnaissance in nature this study has characterized the major gas chemistry features of the Creede hydrothermal system. Gas chemistry studies can be powerful indicators of sources and evolution of fluids. Gas chemistry data also show exceptional promise as indicators of disequilibrium in hydrothermal systems that in turn can be useful tracers of the hydrology of the system. However, to reach full potential the gas chemistry studies must be combined with detailed paragenetic, fluid inclusion, and stable isotope studies. Finally, the techniques used here illustrate the potential to make quantitative distinctions of gas chemistry between multiple populations of fluid inclusion in a single host mineral crystal. The gas data of samples with fluid inclusions susceptible to flushing

by later fluids demonstrates that populations of pseudosecondary and secondary fluid inclusions are not "yesterday's tap water" but can contain fluids present in the system during and just subsequent to ore-forming processes and can be important to understanding the hydrologic history of the system.

The gas chemical composition of the Creede system was highly variable in time and space. Different fluid sources had different gas chemistries which were modified by deep rock interaction and shallow mixing and/or boiling processes. In addition, organic matter from different sources underwent different degrees of degradation and place important constraints on the hydrology of the system. The existence of significant disequilibrium amounts of SO_2 indicate that metastable thiosulfate formed during the mixing of hydrothermal fluids with overlying low pH waters during main stage mineralization and especially during the collapse of the hydrothermal system.

REFERENCES CITED

Bethke, P. M., 1987, The Creede ore-forming system: A summary model: U.S.Geol.Survey Open-File Reports 88-403, 29 p.

Barton, P. B., Jr., Bethke, P.M., and Roedder, E., 1977, Environment of ore deposition in the Creede Mining district, San Juan Mountains, Colorado: Part III. Progress toward interpretation of the chemistry of the ore-forming fluid for the OH vein: Econ. Geol., v. 72, p. 1-24.

Barton, P. B., Jr., 1987, The role of archetypes in understanding ore genesis: Lessons form Creede [abs.]: Geol. Soc. America Abstracts with Programs, v. 19, no. 5, p. 259.

Foley, N.K., Bethke, P.M., and Rye, R.O., 1982, A re-interpretation of δD_{H2O} values of inclusion fluids in quartz from shallow ore deposits [abs.]: Geo. Soc, America Abstracts with Programs, v.14, p. 489.

Foley, N. K., Barton, P. B., Jr., Bethke, P. M., and Doe, B. R., 1987, The isotopic composition of ore lead in the Creede mining district and vicinity, San Juan Mountains, Colo. [abs.]: Geol. Soc. America Abstracts with Programs, v. 19, no. 5, p. 275.

Foley, N.K., Bethke, P.M., and Rye, R.O., 1990, A re-interpretation of δD_{H2O} of inclusion fluids in quartz and sphalerite, Creede mining district, Colorado: a generic problem for shallow ore deposits?: Econ. Geol., (in press).

Hayba, D. O., 1987, Fluid-inclusion evidence for hydrologic and hydrothermal processes in the Creede mineralizing system, Colorado [abs.]: Geol. Soc. America Abstracts with Programs, v. 19, no. 5, p. 282.

Hayba, D. O., Bethke, P. M., Foley, N. K., and Heald, P., 1985, Geologic, mineralogic, and geochemical characteristics of volcanic-hosted epithermal precious-metal deposits: in Geology and Geochemistry of epithermal systems (Berger, B., and Bethke, P. M., eds.), Reviews in Econ. Geol., v. 2, p. 129-167.

Landis, G. P. and Rye, R. O., 1987, Reconnaissance gas chemistry of the Creede, Colorado, hydrothermal system [abs]: Geol. Soc. America Abstracts with Programs, v. 19, no. 5, p. 288.

Plumlee, G. S., Barton, P. B., Jr., and Rye, R. O., 1989, Diverse chemical processes in a complex epithermal system: a progress report from Creede, Colorado: U.S.Geol.Survey Open-File Reports 89-90, 23 p.

Plumlee, G. S., and Rye, R. O., 1989, Mineralization in the waning Creede epithermal system and similar behavior in other systems: U.S.Geol. Survey Open-File Report 89-95, 30 p.

Rye, R. O., Plumlee, G. S., Bethke, P. M., and Barton, P. B., Jr., 1987, Stable isotope geochemistry of the Creede, Colorado, hydrothermal system: U.S. Geol. Survey Open-File Reports 88-356, 40 p.

Steven, T.A. and Eaton G.P., 1975, Environment of ore deposition in the Creede mining district, San Juan Mountains, Colorado I. Geologic, hydrologic, and geophysical setting: Econ. Geol., v. 70, p. 1023-1037.

SCHEMATIC DIAGRAM OF QUADRUPOLE MASS SPECTROMETER

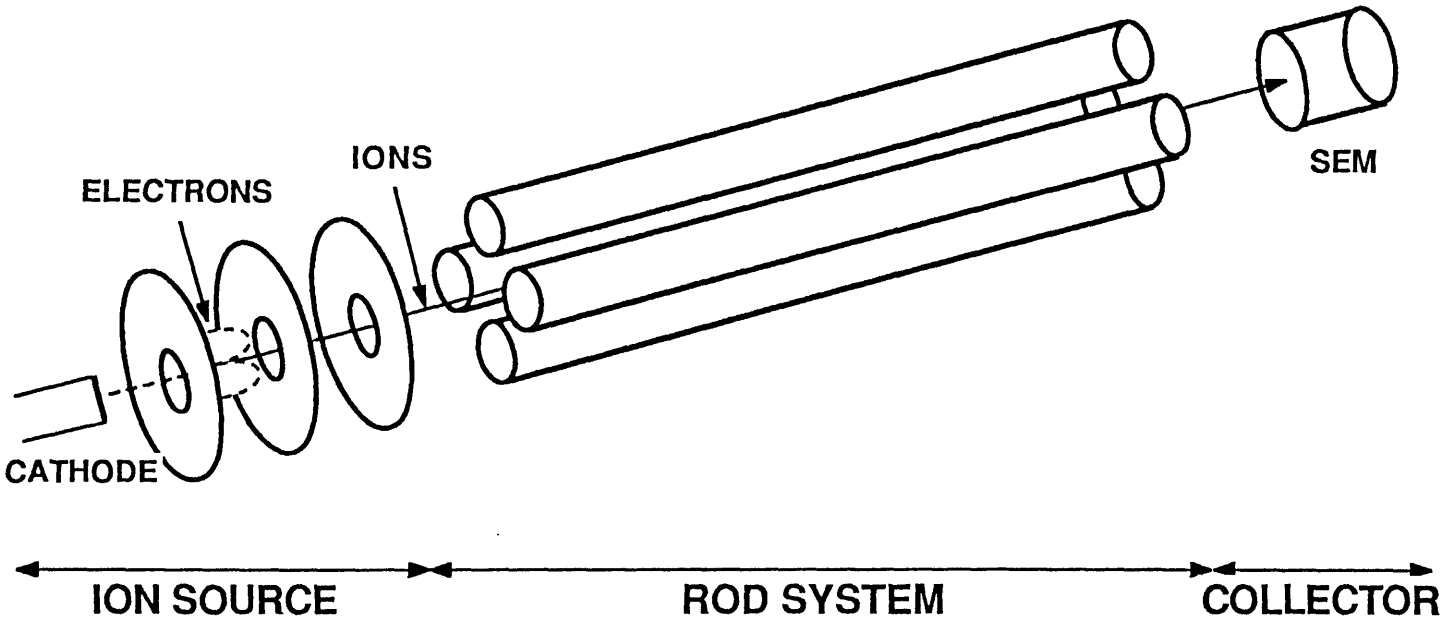

FIGURE 1

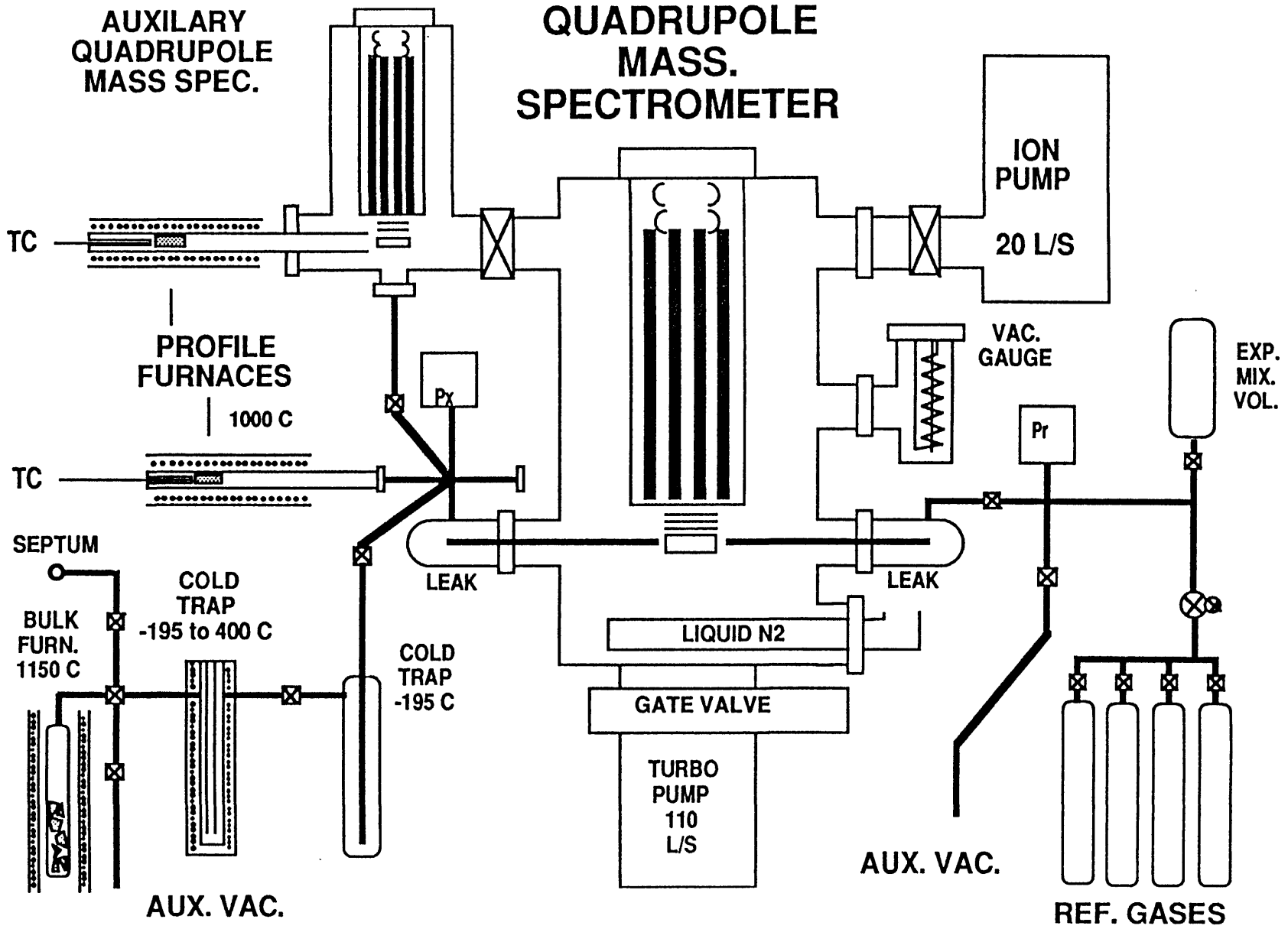
AUXILARY
QUADRUPOLE
MASS SPEC.
QUADRUPOLE
MASS.
SPECTROMETER
ION
PUMP
20 L/S
TC
PROFILE
FURNACES
1000 C
TC
Px
VAC.
GAUGE
EXP.
MIX.
VOL.
Pr
SEPTUM
COLD
TRAP
-195 to 400 C
BULK
FURN.
1150 C
COLD
TRAP
-195 C
LEAK
LEAK
LIQUID N2
GATE VALVE
TURBO
PUMP
110
L/S
AUX. VAC.
AUX. VAC.
REF. GASES

FIGURE 2

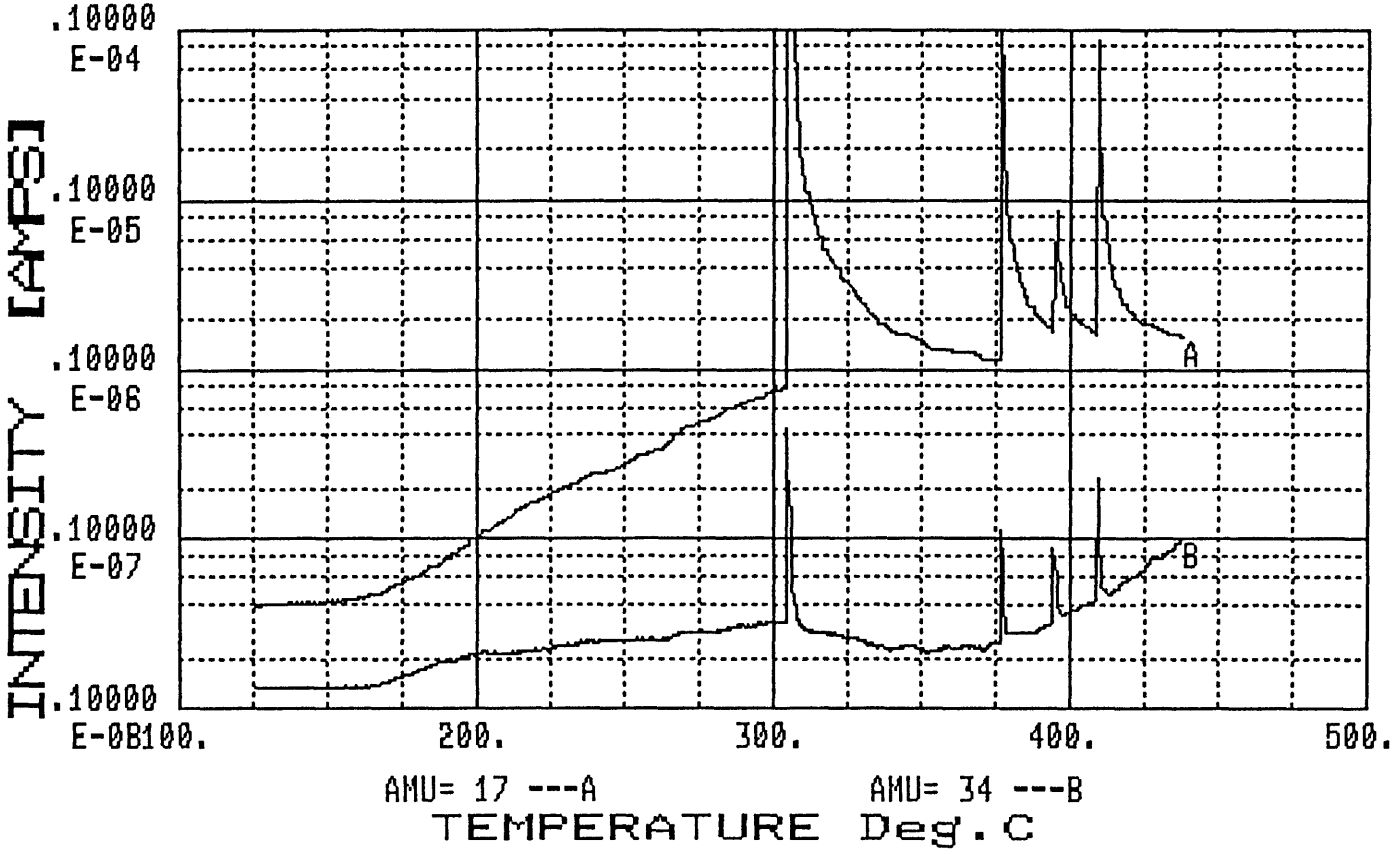
DU1:Q0234R.MIM
.10000
E-04
.10000
E-05
.10000
E-06
.10000
E-07
.10000
E-0B
INTENSITY [AMPS]
100.
200.
300.
400.
500.
A
B
AMU= 17 ---A
AMU= 34 ---B
TEMPERATURE Deg.C

FIGURE 3

MASS SPECTRUM DATA REDUCTION

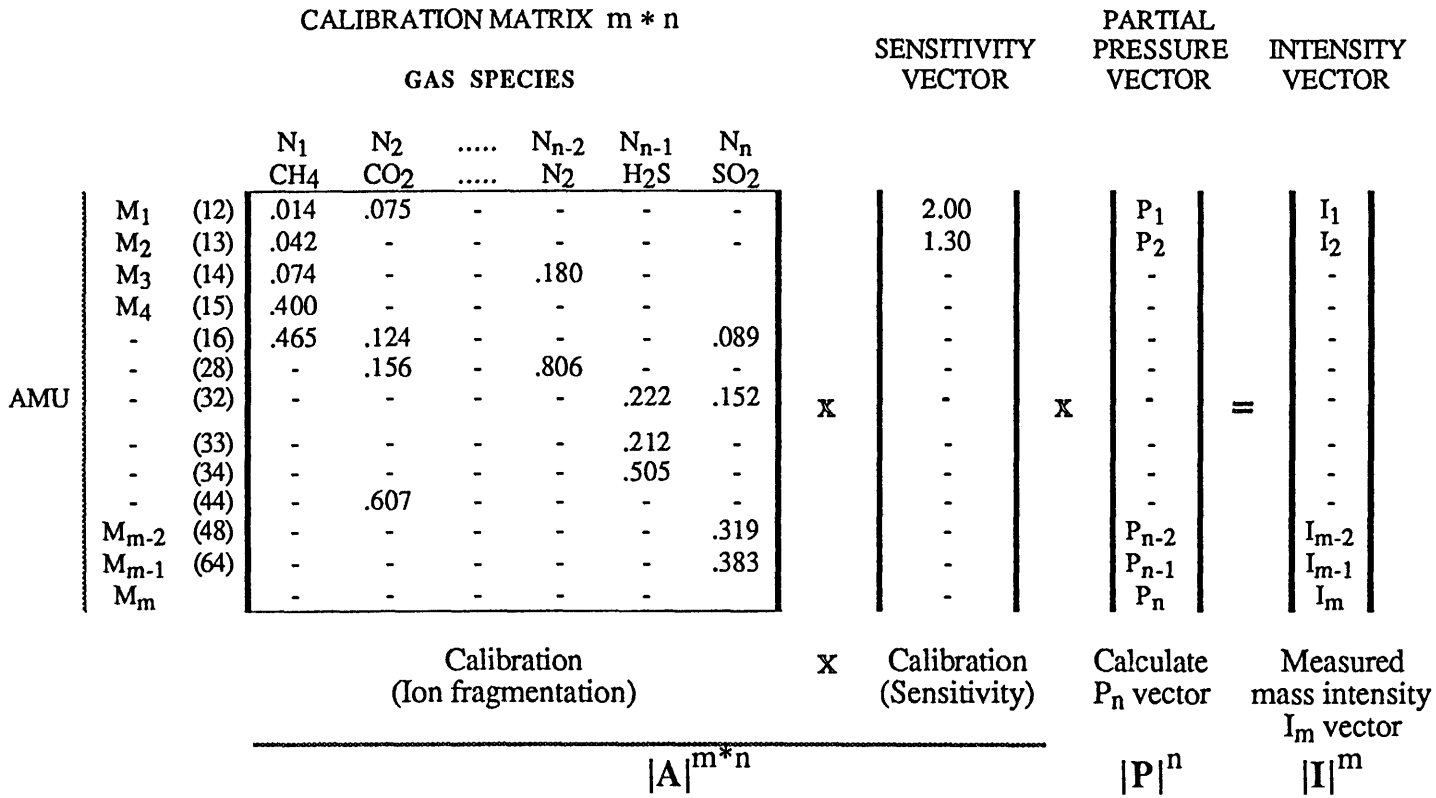

MATRIX SOLUTION

$$|A|^{m*n} * |P|^{n} = |I|^{m}$$

$$|P|^{n} = Q^{-1} * A^{T} * |I|^{m}$$

FIGURE 4

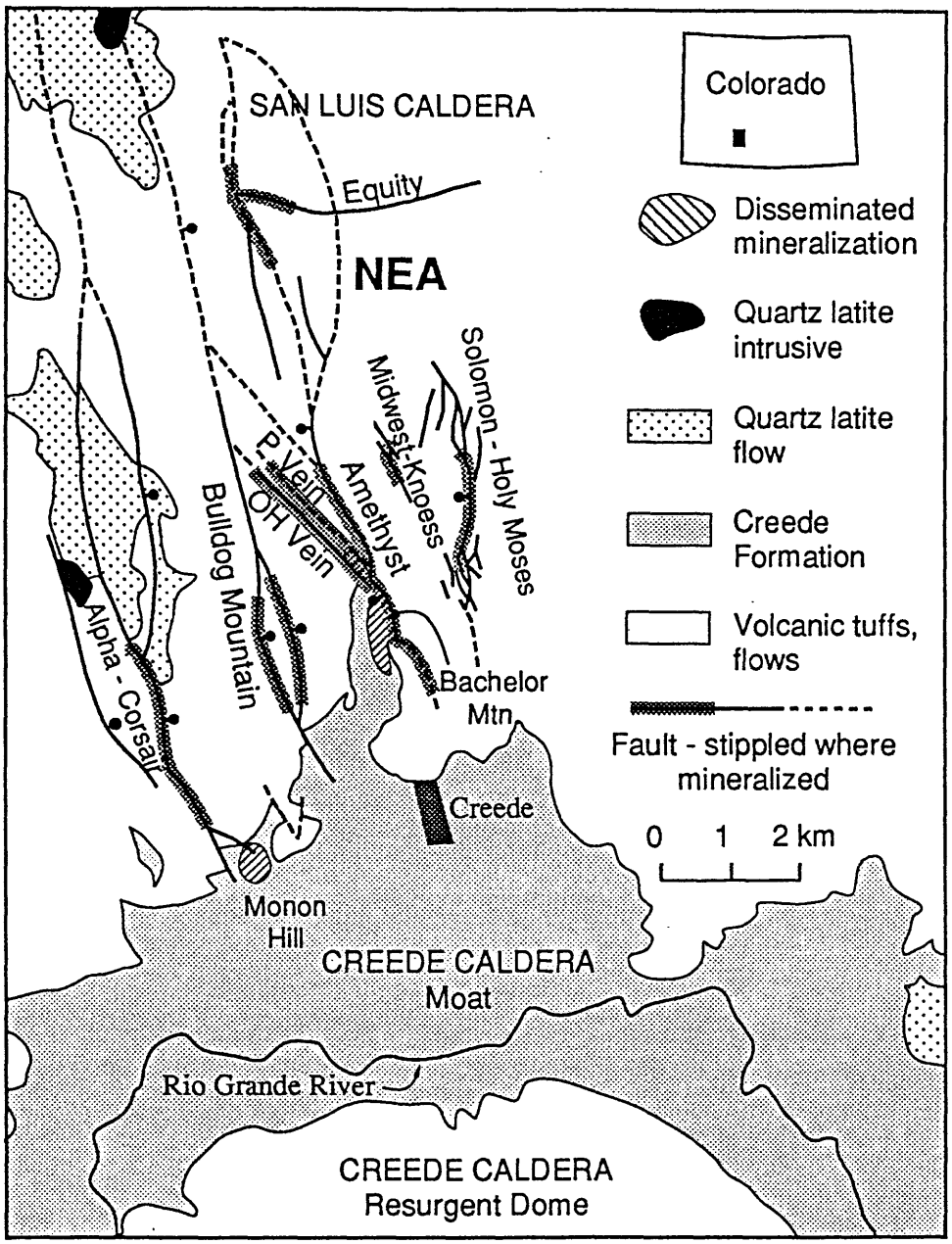
SAN LUIS CALDERA
Equity
NEA
Midwest-Knoess
Solomon - Holy Moses
P. Vein
OH Vein
Amethyst
Bulldog Mountain
Alpha - Corsair
Bachelor Mtn
Creede
Monon Hill
CREEDE CALDERA
Moat
Rio Grande River
CREEDE CALDERA
Resurgent Dome
Colorado
Disseminated mineralization
Quartz latite intrusive
Quartz latite flow
Creede Formation
Volcanic tuffs, flows
Fault - stippled where mineralized
0 1 2 km

FIGURE 5

GAS CHEMISTRY OF THE CREEDE HYDROTHERMAL SYSTEM

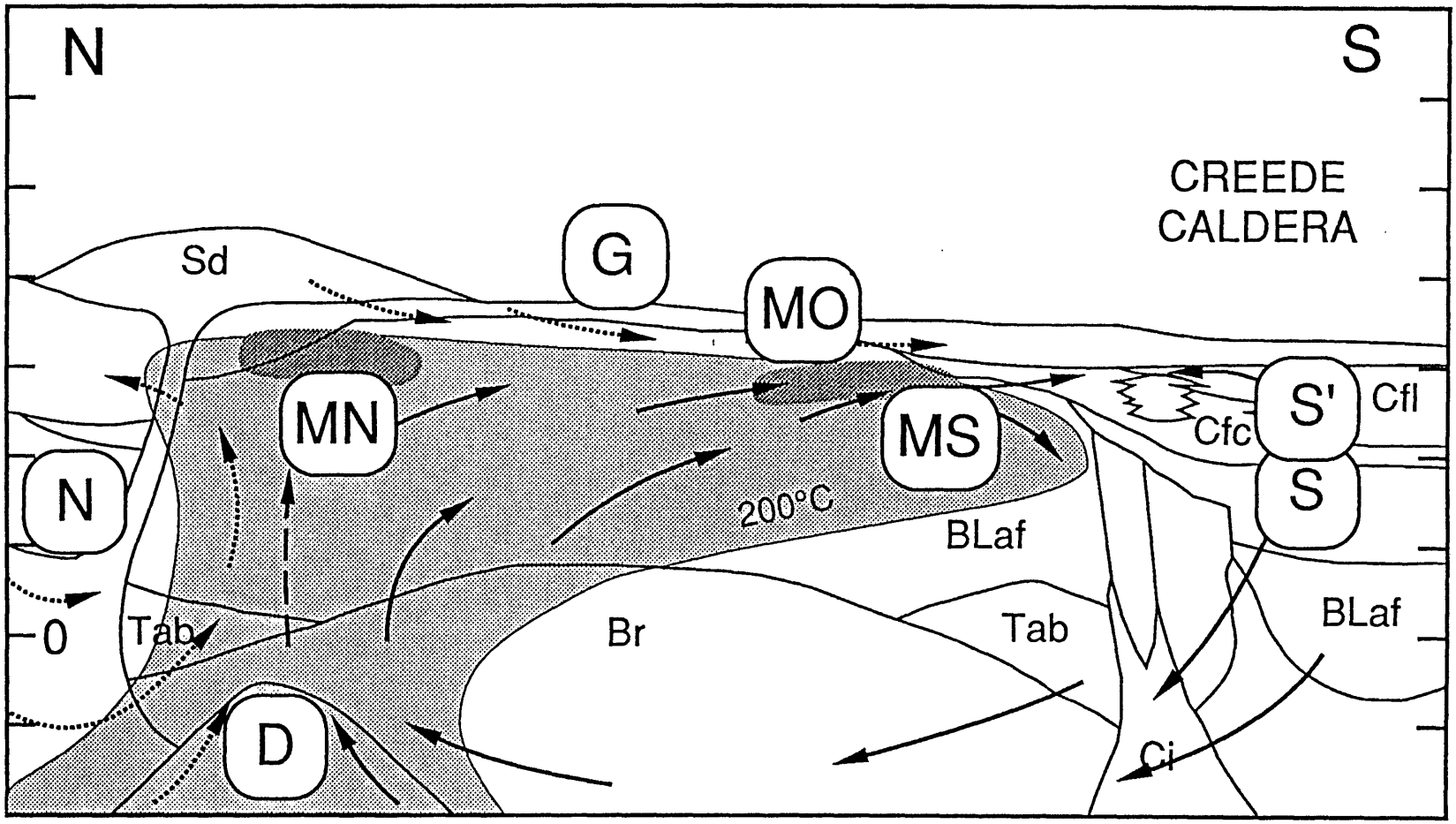

FIGURE 6

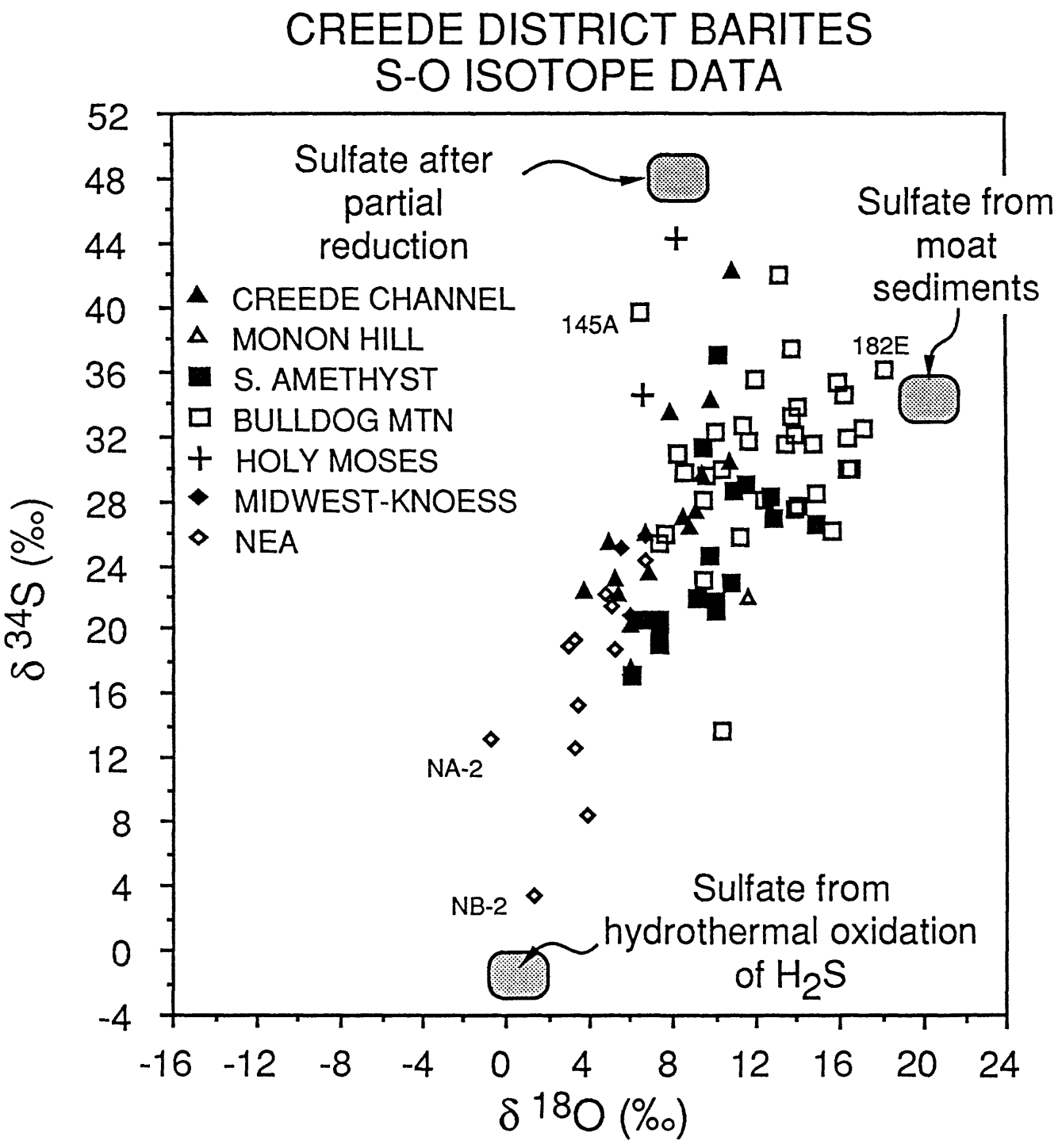
CREEDE DISTRICT BARITES
S-O ISOTOPE DATA
Sulfate after partial reduction
Sulfate from moat sediments
CREEDE CHANNEL
MONON HILL
S. AMETHYST
BULLDOG MTN
HOLY MOSES
MIDWEST-KNOESS
NEA
145A
182E
NA-2
NB-2
Sulfate from hydrothermal oxidation of H2S
δ 34S (‰)
δ 18O (‰)
52
48
44
40
36
32
28
24
20
16
12
8
4
0
-4
-16
-12
-8
-4
0
4
8
12
16
20
24

FIGURE 7

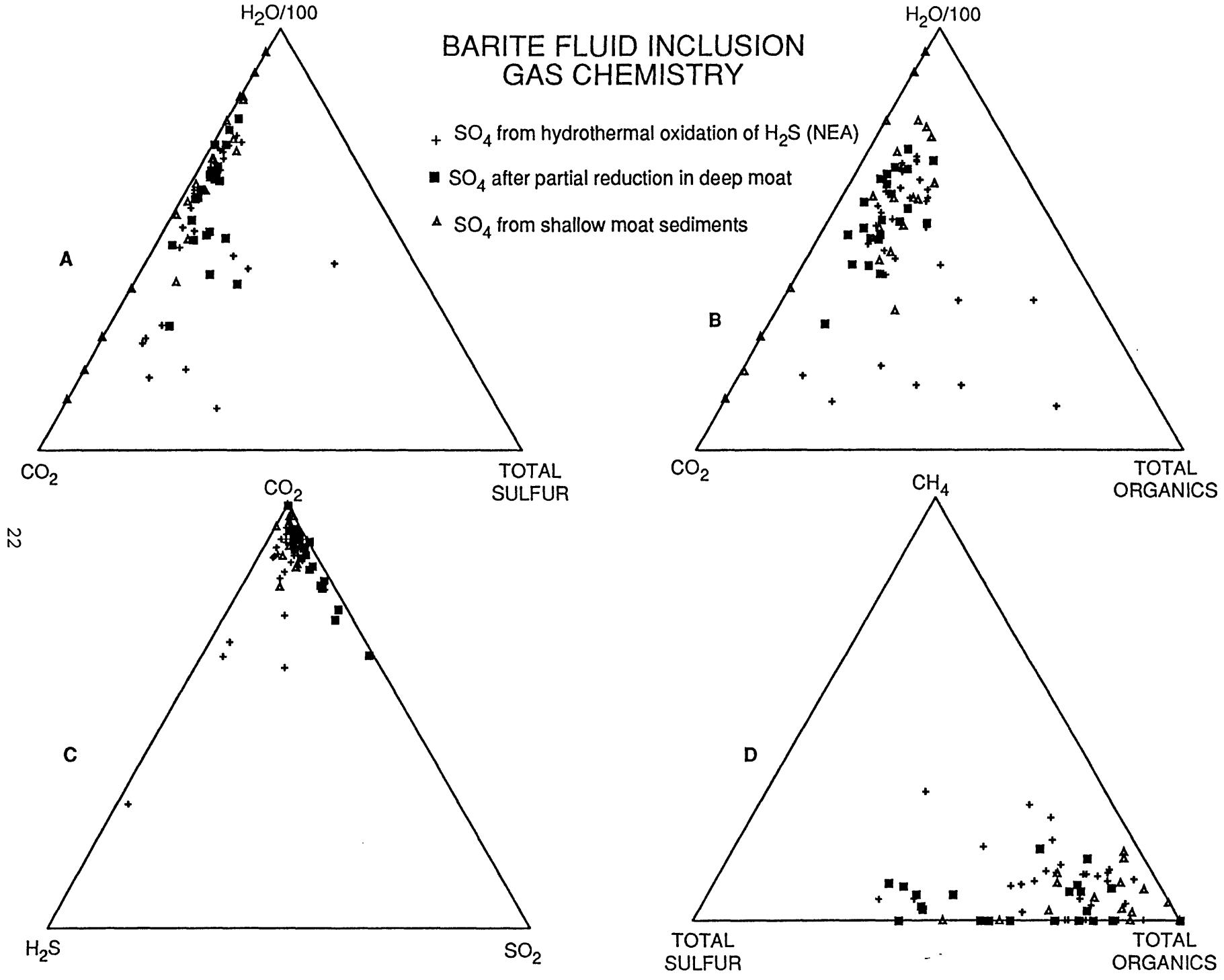
BARITE FLUID INCLUSION
GAS CHEMISTRY
+ SO4 from hydrothermal oxidation of H2S (NEA)
■ SO4 after partial reduction in deep moat
▲ SO4 from shallow moat sediments
A
H2O/100
CO2
TOTAL SULFUR
B
H2O/100
CO2
TOTAL ORGANICS
C
CO2
H2S
SO2
D
CH4
TOTAL SULFUR
TOTAL ORGANICS

FIGURE 8

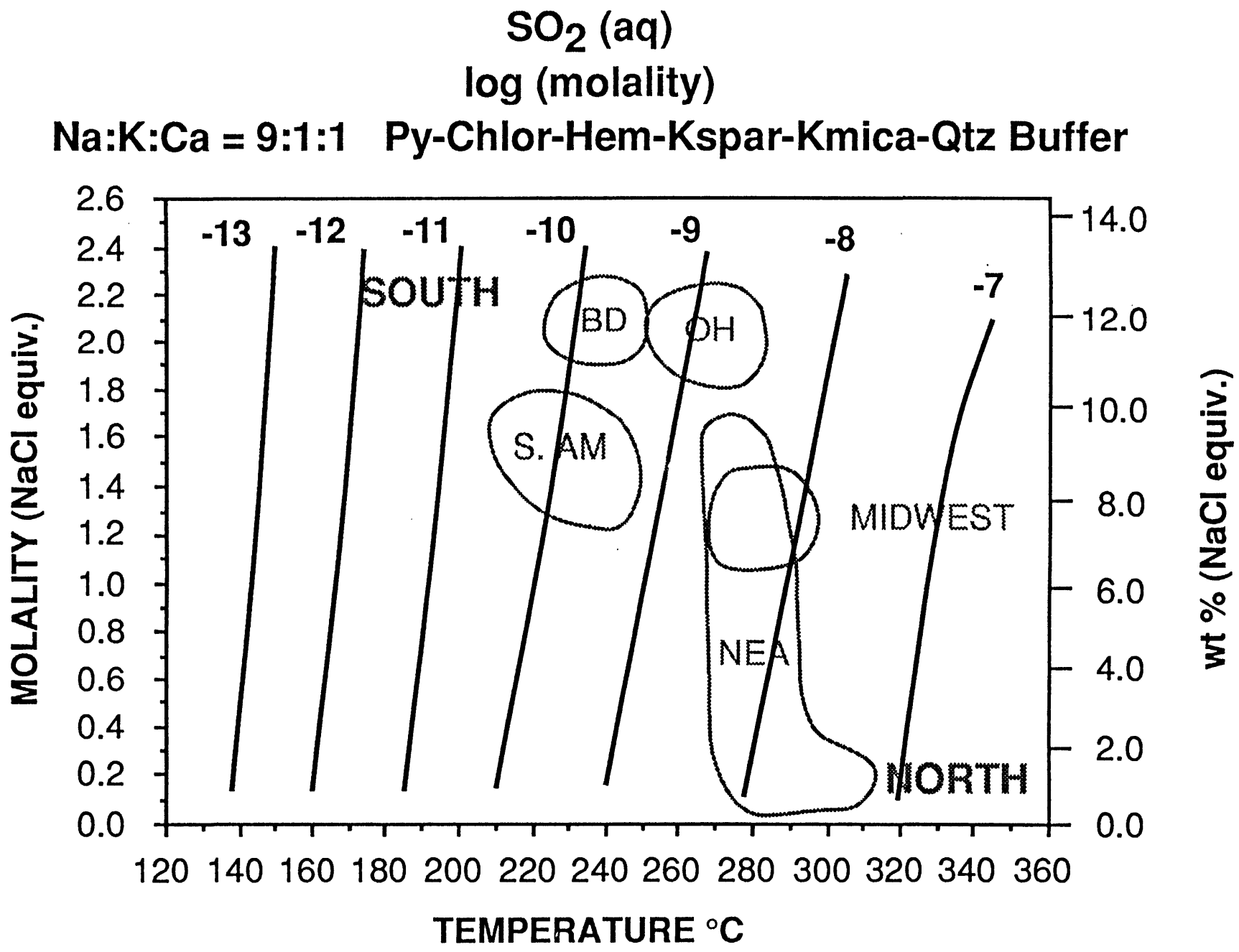
SO_2 (aq)
log (molality)
Na:K:Ca = 9:1:1 Py-Chlor-Hem-Kspar-Kmica-Qtz Buffer
MOLALITY (NaCl equiv.)
wt % (NaCl equiv.)
TEMPERATURE °C
2.6
2.4
2.2
2.0
1.8
1.6
1.4
1.2
1.0
0.8
0.6
0.4
0.2
0.0
14.0
12.0
10.0
8.0
6.0
4.0
2.0
0.0
120 140 160 180 200 220 240 260 280 300 320 340 360
-13
-12
-11
-10
-9
-8
-7
SOUTH
BD
OH
S. AM
MIDWEST
NEA
NORTH

FIGURE 9

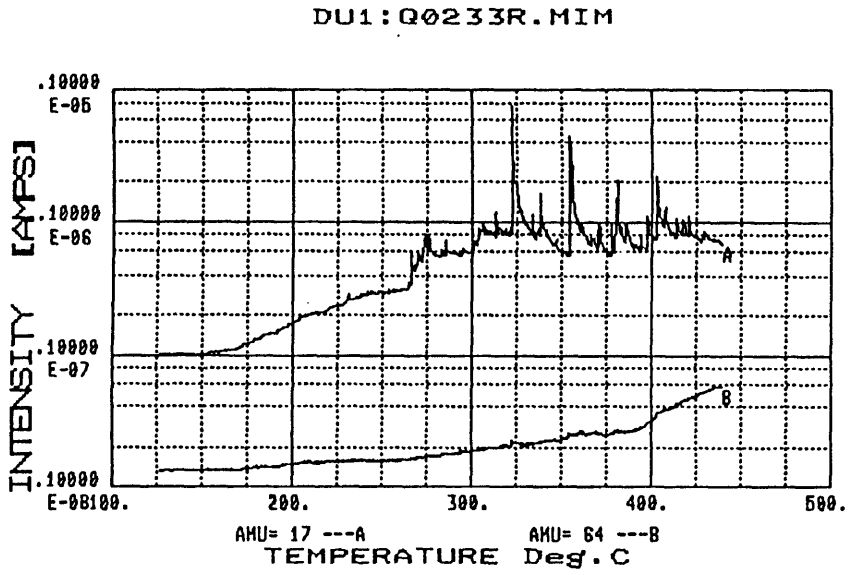
DU1:Q0233R.MIM
.10000
E-05
.10000
E-06
.10000
E-07
.10000
E-08
INTENSITY [AMPS]
100.
200.
300.
400.
500.
A
B
AMU= 17 ---A
AMU= 64 ---B
TEMPERATURE Deg.C

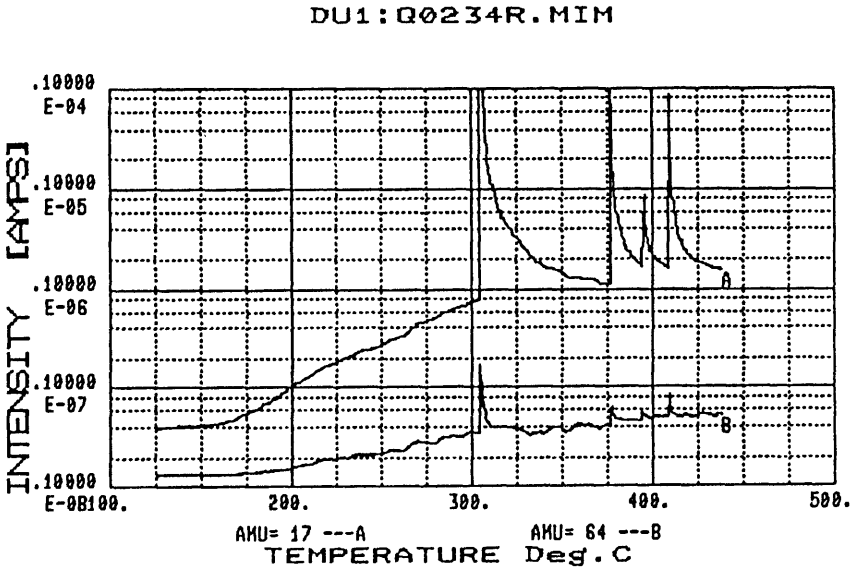
DU1:Q0234R.MIM
.10000
E-04
.10000
E-05
.10000
E-06
.10000
E-07
.10000
E-08
INTENSITY [AMPS]
100.
200.
300.
400.
500.
A
B
AMU= 17 ---A
AMU= 64 ---B
TEMPERATURE Deg.C

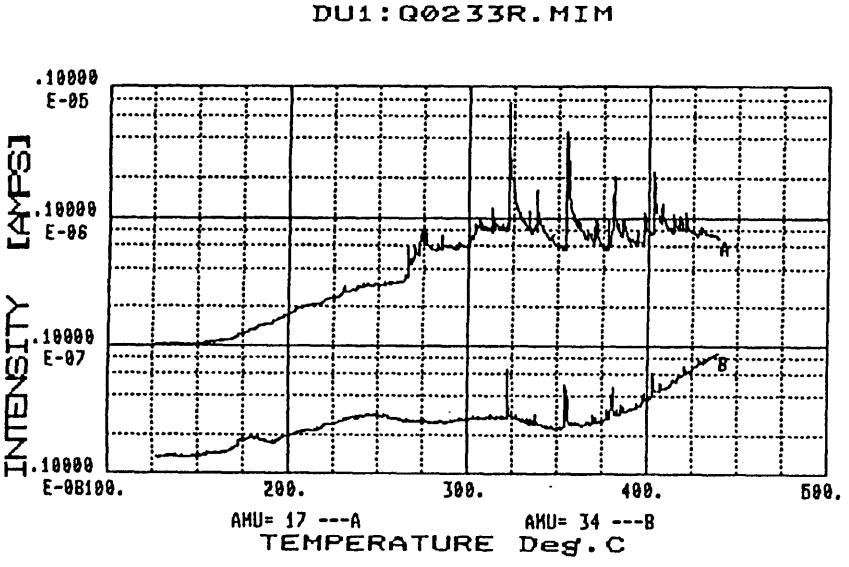
DU1:Q0233R.MIM
.10000
E-05
.10000
E-06
.10000
E-07
.10000
E-08
INTENSITY [AMPS]
100.
200.
300.
400.
500.
A
B
AMU= 17 ---A
AMU= 34 ---B
TEMPERATURE Deg.C

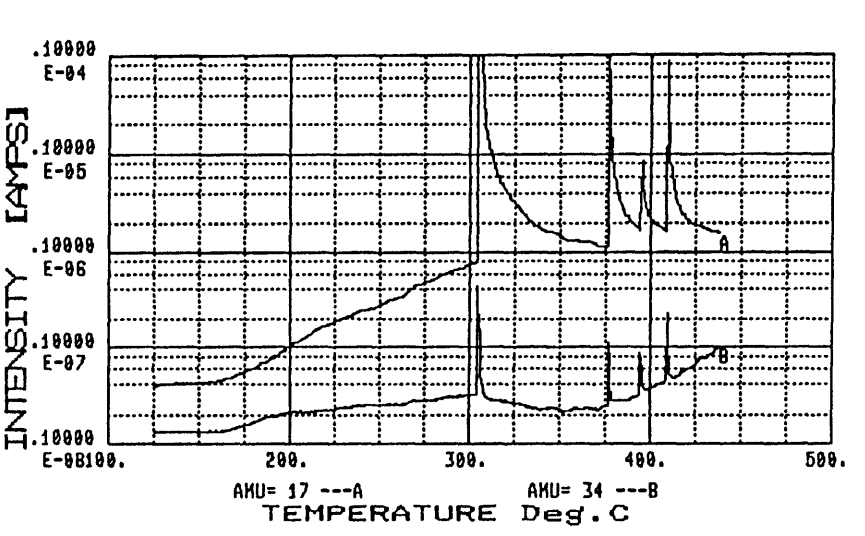
DU1:Q0234R.MIM
.10000
E-04
.10000
E-05
.10000
E-06
.10000
E-07
.10000
E-08
INTENSITY [AMPS]
100.
200.
300.
400.
500.
A
B
AMU= 17 ---A
AMU= 34 ---B
TEMPERATURE Deg.C

FIGURE 10

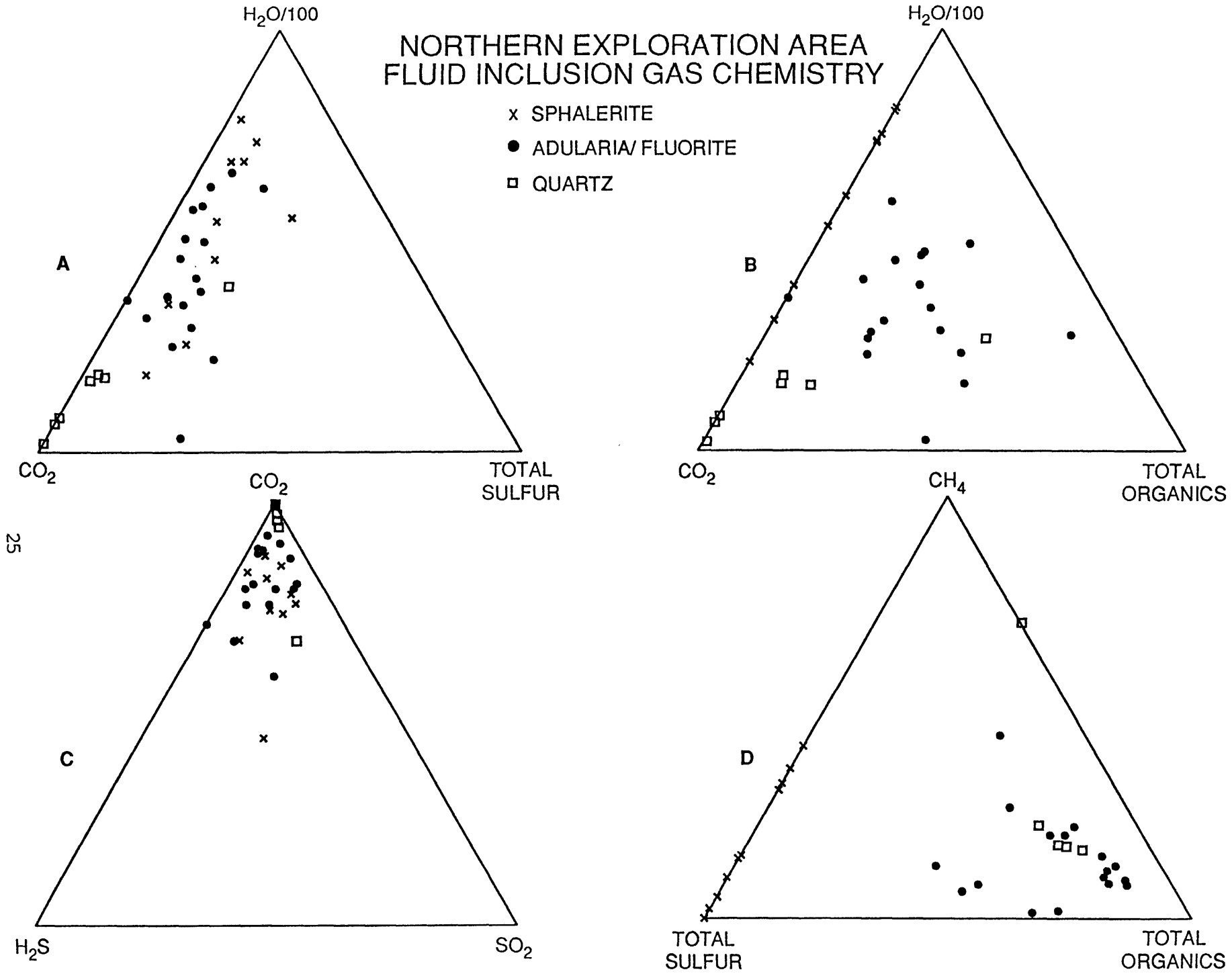
NORTHERN EXPLORATION AREA
FLUID INCLUSION GAS CHEMISTRY
x SPHALERITE
● ADULARIA/ FLUORITE
□ QUARTZ
A
$H_2O/100$
CO_2
TOTAL SULFUR
B
$H_2O/100$
CO_2
TOTAL ORGANICS
C
CO_2
H_2S
SO_2
D
CH_4
TOTAL SULFUR
TOTAL ORGANICS

FIGURE 11

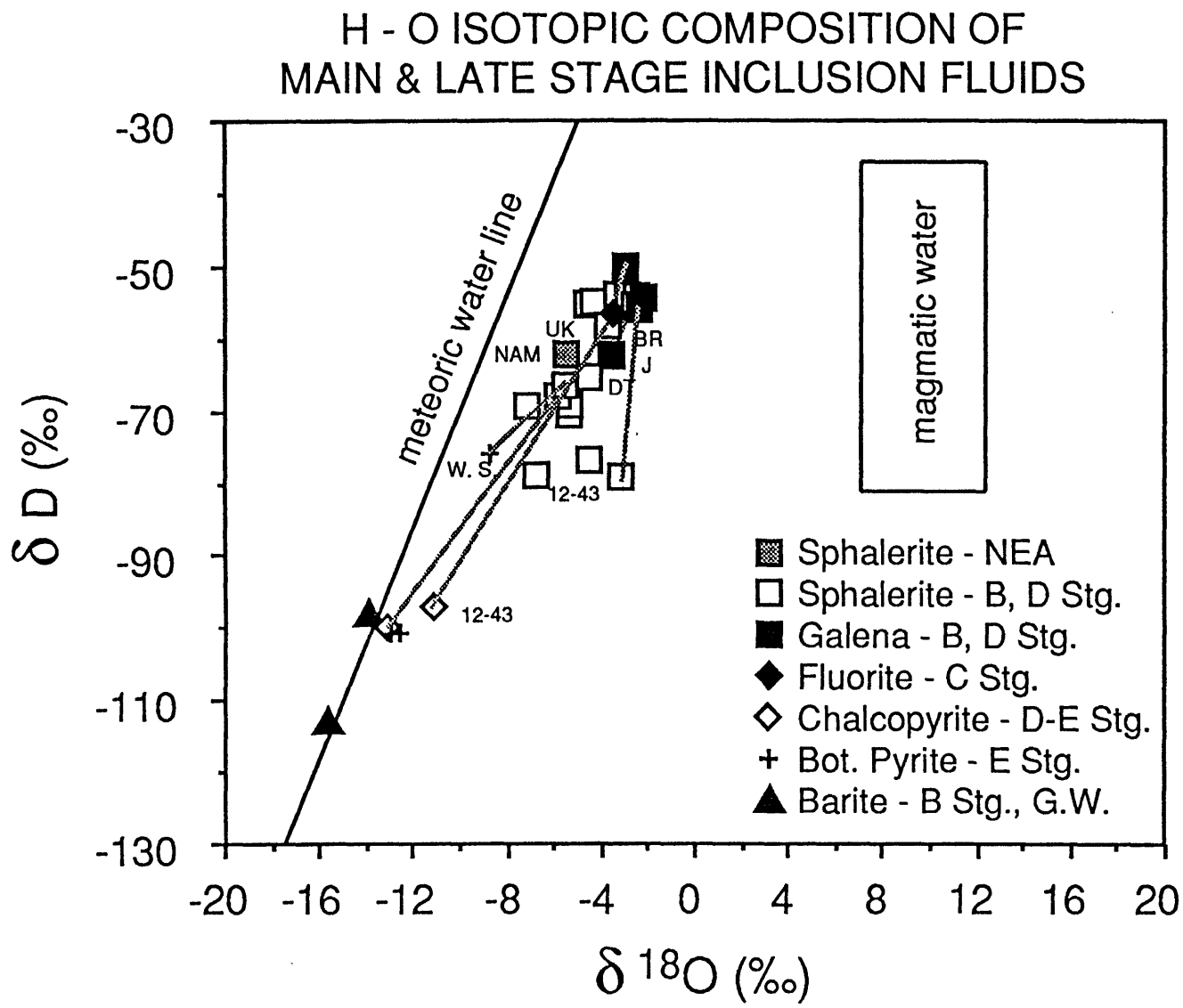
H - O ISOTOPIC COMPOSITION OF
MAIN & LATE STAGE INCLUSION FLUIDS
meteoric water line
magmatic water
UK
NAM
BR
J
D
W. S.
12-43
12-43
Sphalerite - NEA
Sphalerite - B, D Stg.
Galena - B, D Stg.
Fluorite - C Stg.
Chalcopyrite - D-E Stg.
Bot. Pyrite - E Stg.
Barite - B Stg., G.W.
δ D (‰)
-30
-50
-70
-90
-110
-130
-20 -16 -12 -8 -4 0 4 8 12 16 20
δ 18O (‰)

FIGURE 12

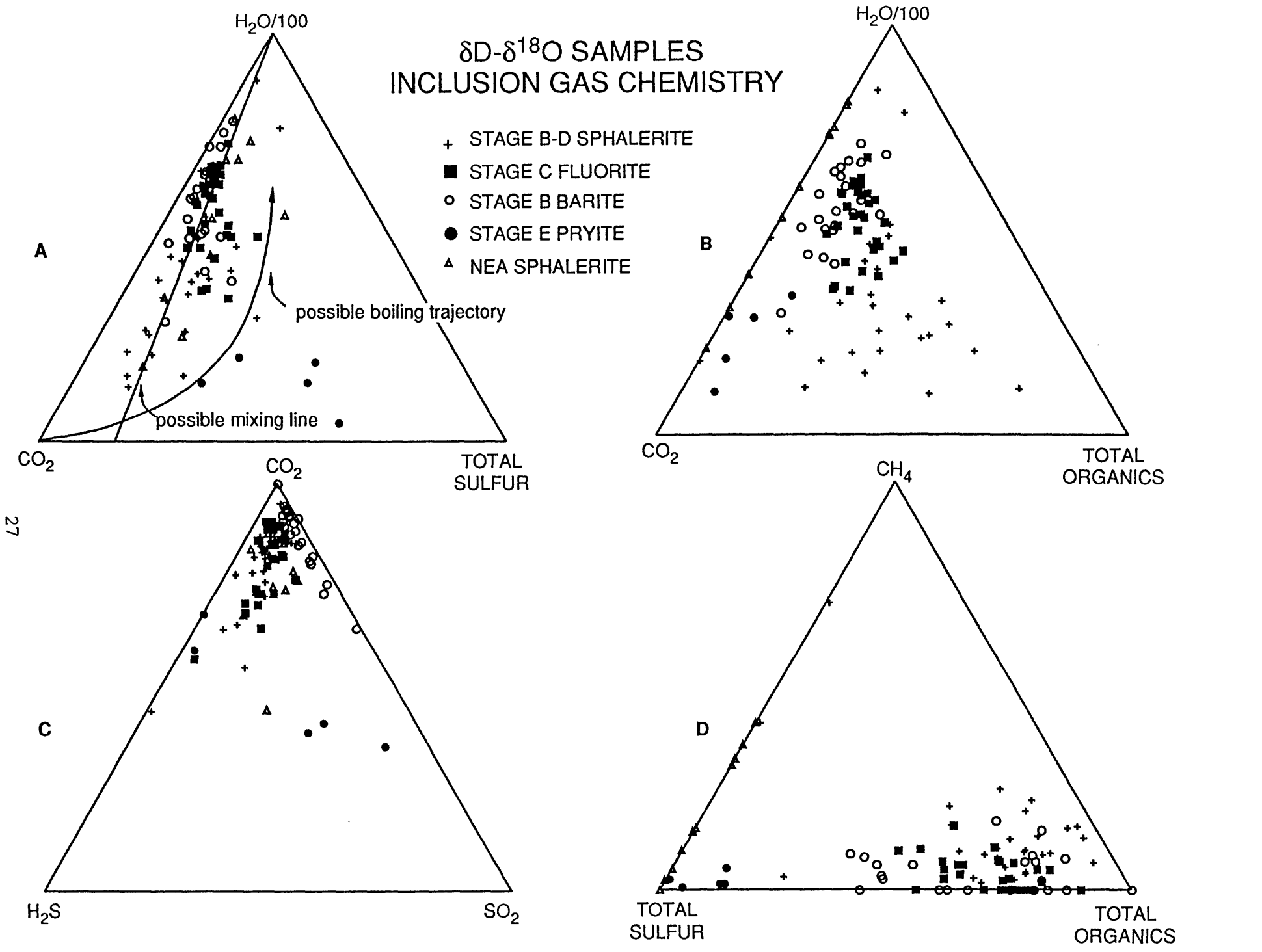
δD-δ18O SAMPLES
INCLUSION GAS CHEMISTRY
+ STAGE B-D SPHALERITE
■ STAGE C FLUORITE
○ STAGE B BARITE
● STAGE E PRYITE
△ NEA SPHALERITE
A
H2O/100
CO2
TOTAL SULFUR
possible boiling trajectory
possible mixing line
B
H2O/100
CO2
TOTAL ORGANICS
C
CO2
H2S
SO2
D
CH4
TOTAL SULFUR
TOTAL ORGANICS

FIGURE 13

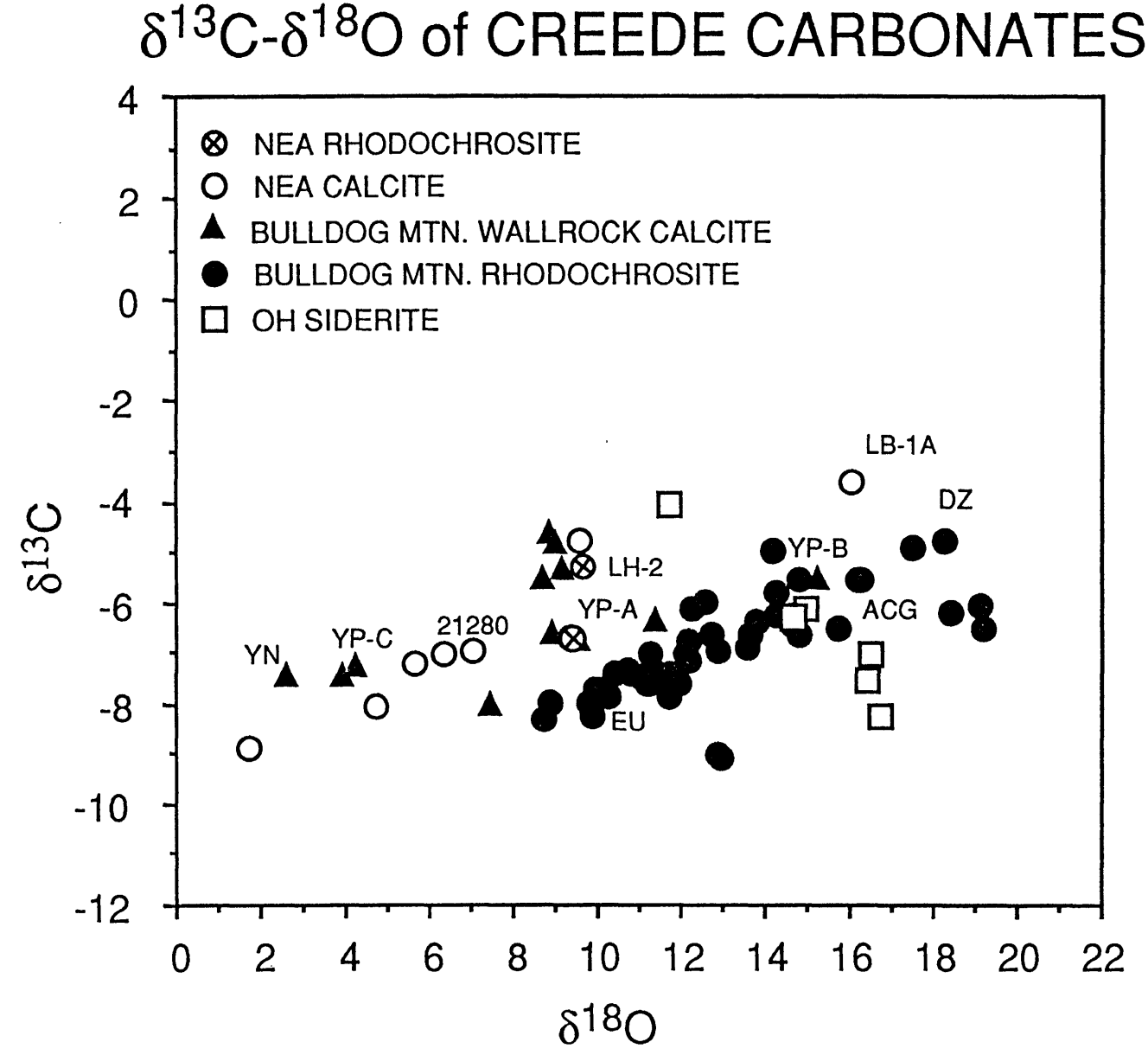
δ13C-δ18O of CREEDE CARBONATES
NEA RHODOCHROSITE
NEA CALCITE
BULLDOG MTN. WALLROCK CALCITE
BULLDOG MTN. RHODOCHROSITE
OH SIDERITE
LB-1A
DZ
YP-B
LH-2
YP-A
ACG
21280
YP-C
YN
EU
δ13C
δ18O
4
2
0
-2
-4
-6
-8
-10
-12
0
2
4
6
8
10
12
14
16
18
20
22

FIGURE 14

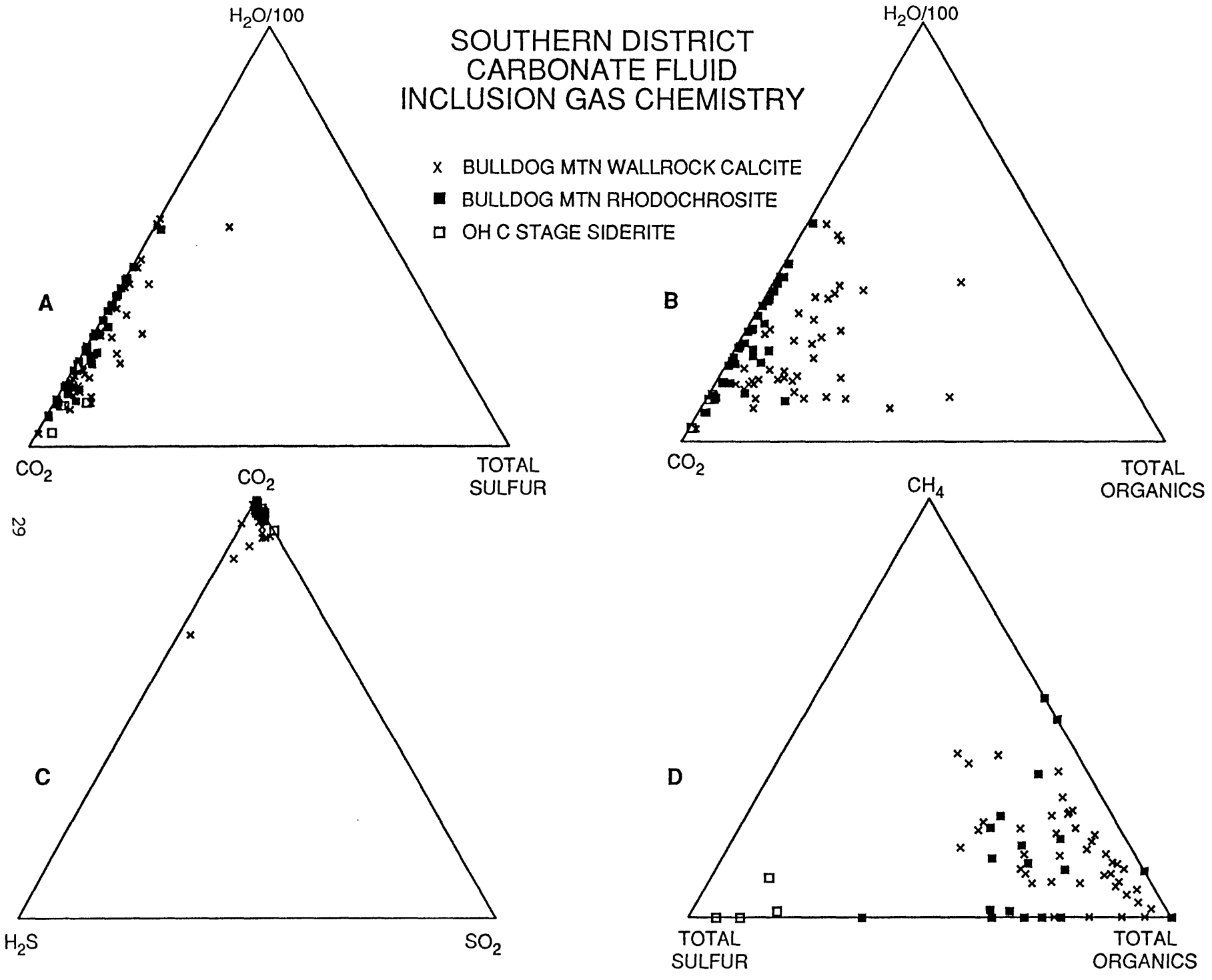
SOUTHERN DISTRICT
CARBONATE FLUID
INCLUSION GAS CHEMISTRY
BULLDOG MTN WALLROCK CALCITE
BULLDOG MTN RHODOCHROSITE
OH C STAGE SIDERITE
A
$H_2O/100$
CO_2
TOTAL SULFUR
B
$H_2O/100$
CO_2
TOTAL ORGANICS
C
CO_2
H_2S
SO_2
D
CH_4
TOTAL SULFUR
TOTAL ORGANICS

FIGURE 15

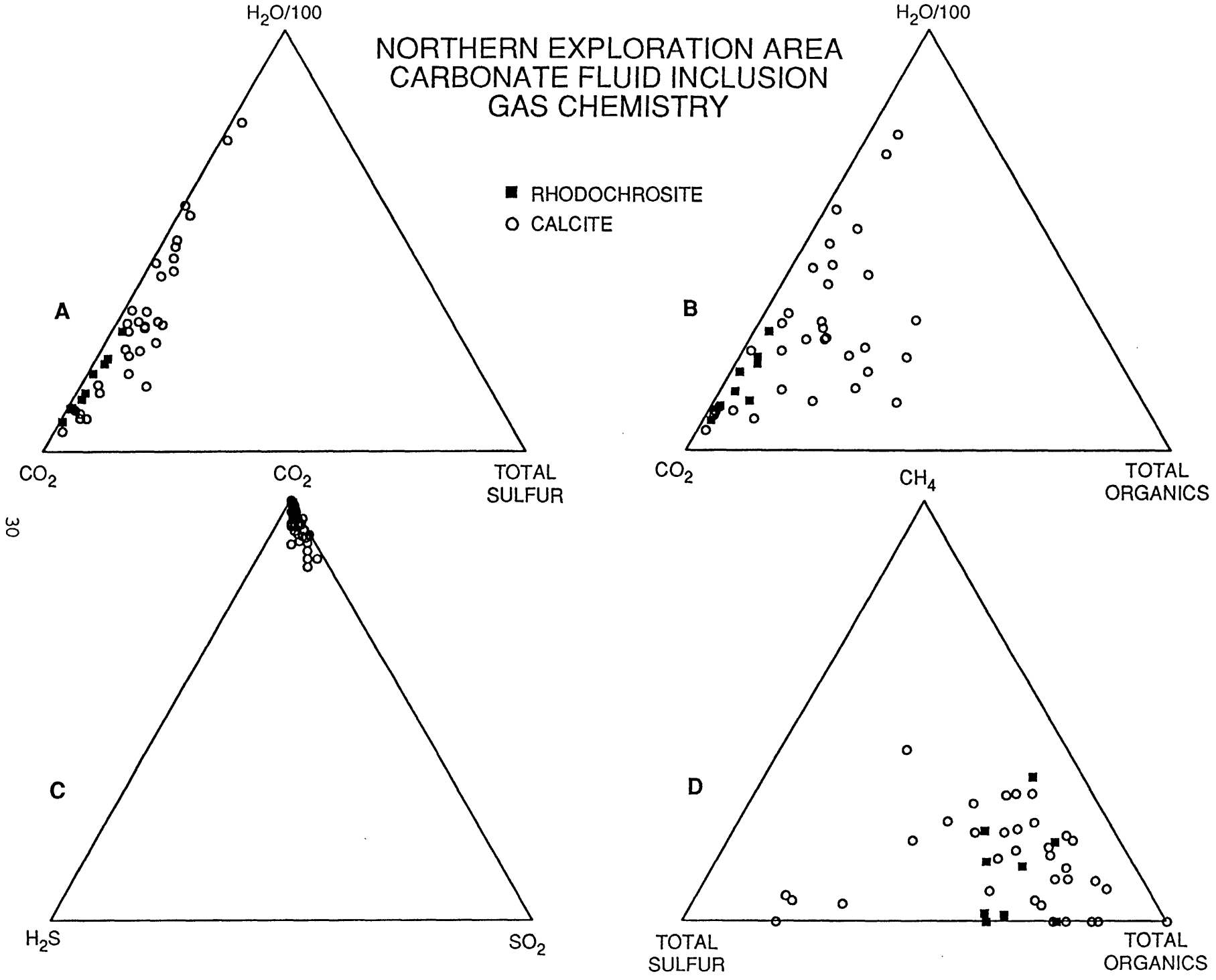
NORTHERN EXPLORATION AREA
CARBONATE FLUID INCLUSION
GAS CHEMISTRY
RHODOCHROSITE
CALCITE
A
$H_2O/100$
CO_2
CO_2
TOTAL SULFUR
B
$H_2O/100$
CO_2
CH_4
TOTAL ORGANICS
C
H_2S
SO_2
D
TOTAL SULFUR
TOTAL ORGANICS

FIGURE 16

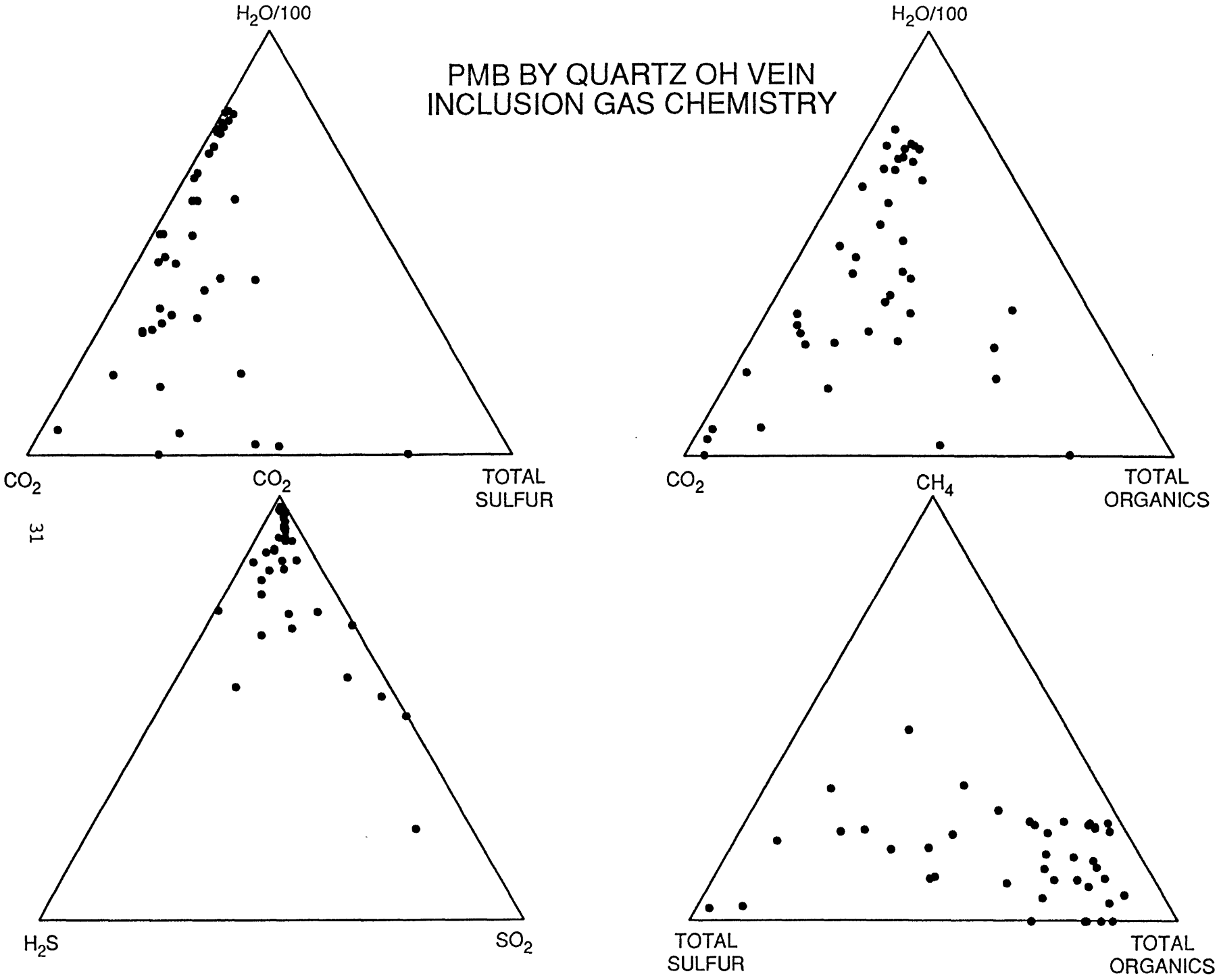
PMB BY QUARTZ OH VEIN
INCLUSION GAS CHEMISTRY
$H_2O/100$
CO_2
CO_2
TOTAL SULFUR
$H_2O/100$
CO_2
CH_4
TOTAL ORGANICS
H_2S
SO_2
TOTAL SULFUR
TOTAL ORGANICS

FIGURE 17

ORGANIC GAS COMPOSITIONS OF CREEDE INCLUSION FLUIDS

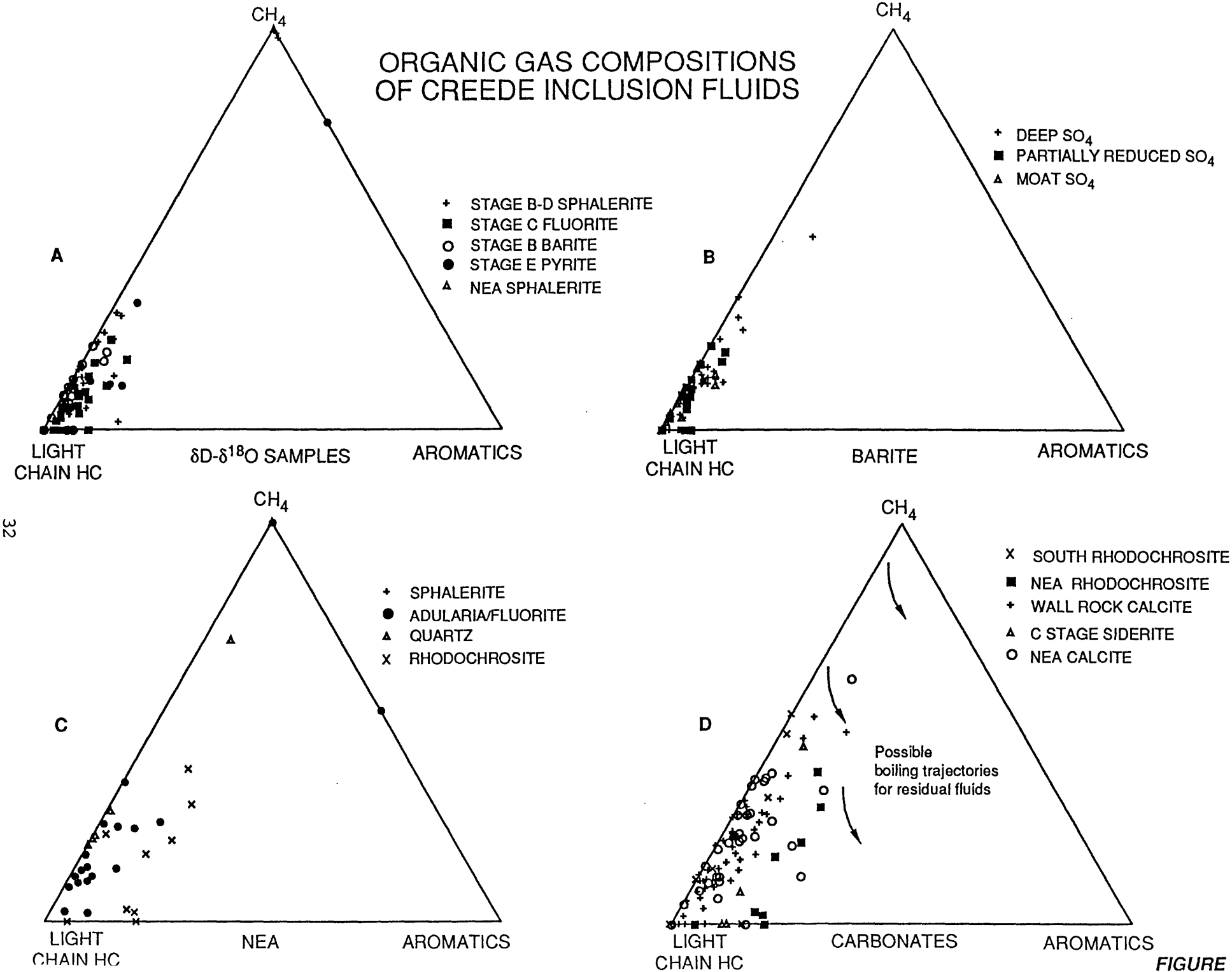

FIGURE 18

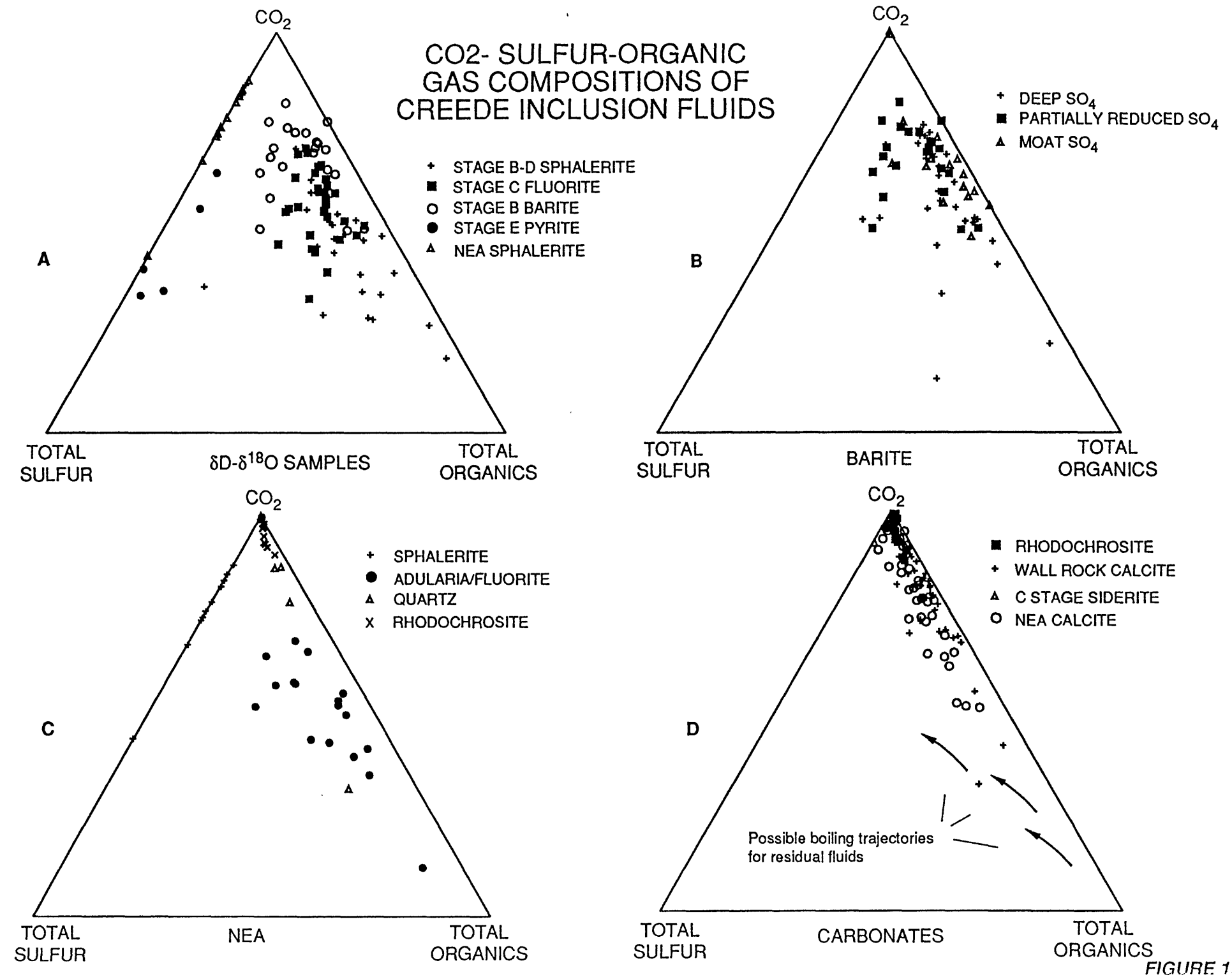
CO2- SULFUR-ORGANIC GAS COMPOSITIONS OF CREEDE INCLUSION FLUIDS
A
CO2
TOTAL SULFUR
δD-δ18O SAMPLES
TOTAL ORGANICS
STAGE B-D SPHALERITE
STAGE C FLUORITE
STAGE B BARITE
STAGE E PYRITE
NEA SPHALERITE
B
CO2
TOTAL SULFUR
BARITE
TOTAL ORGANICS
DEEP SO4
PARTIALLY REDUCED SO4
MOAT SO4
C
CO2
TOTAL SULFUR
NEA
TOTAL ORGANICS
SPHALERITE
ADULARIA/FLUORITE
QUARTZ
RHODOCHROSITE
D
CO2
TOTAL SULFUR
CARBONATES
TOTAL ORGANICS
RHODOCHROSITE
WALL ROCK CALCITE
C STAGE SIDERITE
NEA CALCITE
Possible boiling trajectories for residual fluids

FIGURE 19

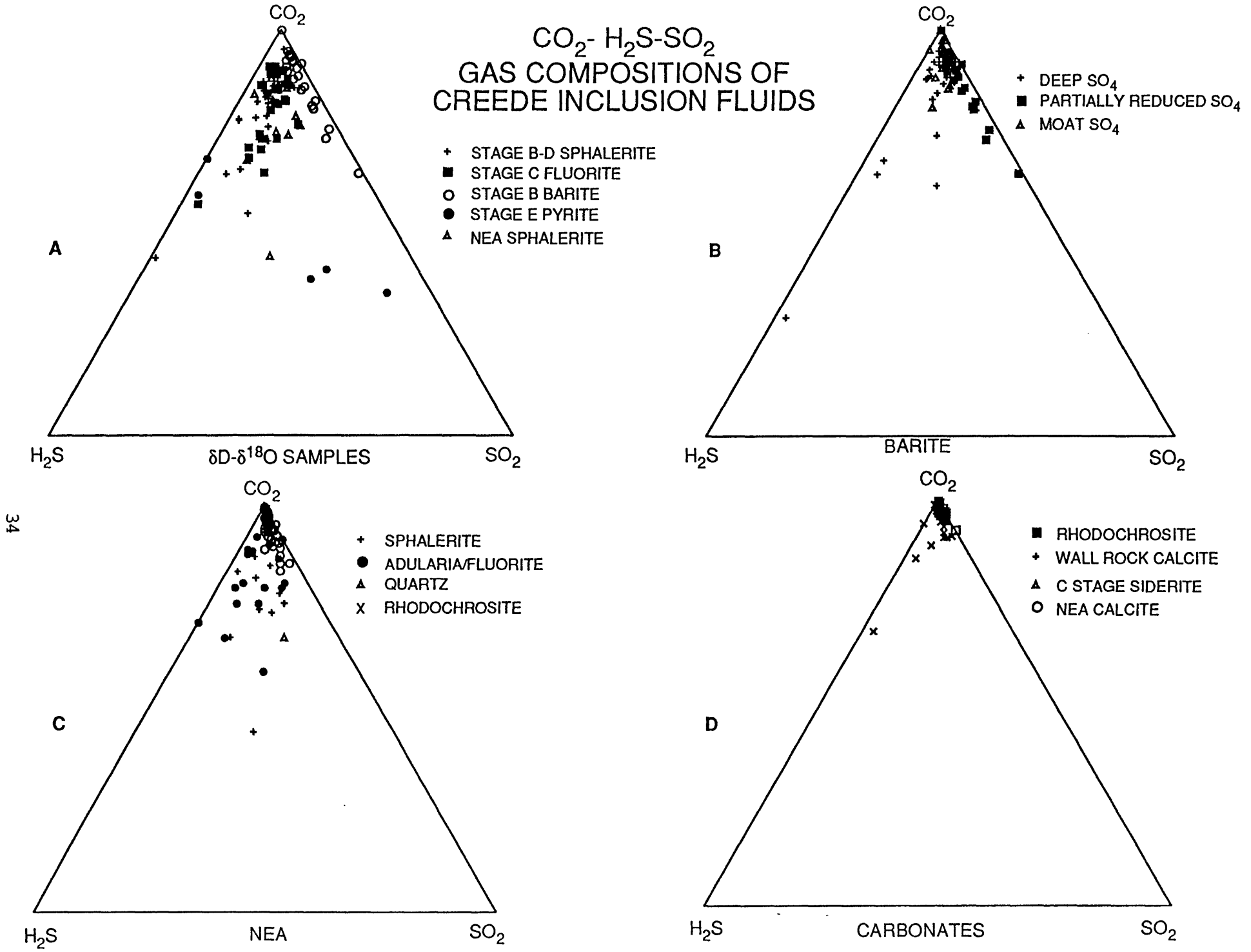
CO_2- H_2S-SO_2
GAS COMPOSITIONS OF
CREEDE INCLUSION FLUIDS
STAGE B-D SPHALERITE
STAGE C FLUORITE
STAGE B BARITE
STAGE E PYRITE
NEA SPHALERITE
A
CO_2
H_2S
δD-$δ^{18}O$ SAMPLES
SO_2
B
CO_2
DEEP SO_4
PARTIALLY REDUCED SO_4
MOAT SO_4
H_2S
BARITE
SO_2
C
CO_2
SPHALERITE
ADULARIA/FLUORITE
QUARTZ
RHODOCHROSITE
H_2S
NEA
SO_2
D
CO_2
RHODOCHROSITE
WALL ROCK CALCITE
C STAGE SIDERITE
NEA CALCITE
H_2S
CARBONATES
SO_2

FIGURE 20

GAS CHEMISTRY OF MAIN FLUID COMPONENTS IN THE CREEDE SYSTEM

FIG. 6	INPUT	CHARACTERISTICS
N:	NORTHERN RECHARGE	CH_4, High-T Organics, NH_3
S:	SOUTHERN RECHARGE (Creede Moat Sediments)	Low-T Organics
D:	DEEP (Magmatic?)	High CO_2, H_2S, HF
G:	OVERLYING GROUNDWATER (Steam-heated, Condensed volatiles)	High CO_2, SO_2
MN:	MIXED (Northern)	CO2>H2S>SO2
MS:	MIXED (Southern)	CO2>H2S=SO2
MO:	MIXED (Overlying)	CO2>SO2>H2S

FIGURE 21

APPENDIX 1: SAMPLES ANALYZED FOR GAS CHEMISTRY OF INCLUSION FLUIDS SHOWING ISOTOPIC INFORMATION ON THE INCLUSION FLUIDS OR THEIR HOST MINERALS

QMS #	FIELD#	MINERAL	LOCATION	STAGE	δD_{H2O}	$\delta^{18}O_{H2O}$	$\delta^{13}C$	$\delta^{18}O$	$\delta^{34}S$
V0224	GSP-KQ-85	QUARTZ	NEA	MAIN	-114				
V0228	NA5-849	QUARTZ	NEA	MAIN	-107				
V0386-0388	GSP-NAM	SPHAL	NEA	MAIN	-66	-5.8			
V0400-0402	GSP-DT	SPHAL	BMV	B	-59	-4.4			
V0414-0415	PBB-12-43-59	CHALCOPY*	OH	E	-107	-13.1			
V0419-0421	PMB-BR-231	SPHAL	OH	D	-57	-3.4			
V0428-0429	PMB-J-47-59	SPHAL	OH	D	-60	-3.6			
V0434-0436	WEST STRAND	PYRITE	BMV	E	-76	-8.7			
V0440-0442	21280 DECLINE	FLUORITE	NEA	LATE					
V0446-0450	PBB-12-43-59	SPHAL	OH	D	-73	-7.2			
V0452-0457	PMB-UK	FLUORITE	BMV	C	-68	-4.4			
V0474-0475	PMB-ADZ-1219-85	ADULARIA	NEA	MAIN					
V0491-0493	PBB-145A	BARITE	BMV	D				6.4	38.8
V0495-0500	PBB-182E	BARITE	BMV	D				18.1	36.5
V0502-0506	NB-2 927'	BARITE	NEA	MAIN				1.2	3.4
V0506-0512	NA-2 712'	BARITE	NEA	MAIN				-0.7	13.2
V0513-0519	PMB-BY-12	QUARTZ	OH	D	-69				
V0582-0583	PMB-YP-1025-79A	CALCITE	BMV	WR			-6.6	8.9	
V0587-0589	PMB-YP-1025-79C	CALCITE	BMV	WR			-7.2	4.2	
V0595-0596	PMB-YP-1025-79B	CALCITE	BMV	WR	-82		-5.5	15.3	
V0629-0630	GSP-DZ-RCIA	RHODO	BMV	A			-4.8	18.2	
V0637-0643	GSP-AN A	RHODO	BMV	A	-73		-8.2	9.8	
V0647-0649	PMB-ACG-1165	RHODO	BMV	A			-5.5	16.2	
V0654-0656	GSP-LH 2	CALCITE	NEA	LATE	-108		-5.3	9.6	
V0660-0661	PBB 110	SIDERITE	OH	C					
V0665-0668	GSP-LB1	RHODO	NEA	EARLY	-119		-0.1	7.6	
V0679	GSP-DZ-RC1A	RHODO	BMV	A			-4.8	18.2	
V0686-0687	PMB-YN	CALCITE	BMV	WR	-76		-7.5	2.6	
V0668-0672	21280 DECLINE	CALCITE	NEA	LATE	-101		-7.1	6.3	

BMV= Bulldog Mountain vein
OH= OH vein
NEA= Northern exploration area
WR= Pre ore wall rock stage
* Fluids are from E stage alteration

APPENDIX 2: GAS CHEMISTRY OF BARITE FLUIDS

Name	V0491A	V0491B	V0492A	V0492B	V0492C	V0492D	V0492E	V0492F	V0492G	V0492H	V0492I	V0492J	V0493A
Deg	261	266	300	305	306	307	308	309	310	311	314	316	333
CH_4	0.000	0.021	0.000	0.006	0.000	0.024	0.020	0.028	0.000	0.043	0.000	0.066	0.000
HF	0.000	0.000	0.000	0.000	0.000	0.000	0.000	0.000	0.000	0.000	0.000	0.000	0.000
N_2	0.070	0.011	0.055	0.101	0.115	0.031	0.082	0.057	0.058	0.000	0.067	0.000	0.038
C_2H_6	0.000	0.000	0.000	0.000	0.000	0.000	0.000	0.000	0.000	0.000	0.000	0.000	0.000
C_3H_8	0.044	0.041	0.131	0.156	0.104	0.138	0.146	0.153	0.118	0.225	0.091	0.193	0.051
H_2S	0.000	0.004	0.000	0.010	0.010	0.018	0.010	0.018	0.008	0.018	0.008	0.010	0.019
HCl	0.000	0.000	0.000	0.000	0.000	0.000	0.000	0.000	0.000	0.000	0.000	0.000	0.000
H_2O	99.435	99.542	99.415	99.020	99.007	99.127	99.409	98.558	99.262	99.015	99.308	98.854	99.208
Ar	0.003	0.004	0.000	0.011	0.005	0.008	0.010	0.018	0.003	0.005	0.003	0.016	0.016
C_5H_{12}	0.000	0.000	0.017	0.036	0.000	0.000	0.063	0.000	0.036	0.000	0.025	0.050	0.024
C_4H_{10}	0.065	0.065	0.000	0.000	0.161	0.113	0.000	0.151	0.000	0.145	0.000	0.000	0.000
SO_2	0.000	0.013	0.032	0.032	0.032	0.049	0.015	0.049	0.032	0.066	0.032	0.067	0.032
CO_2	0.383	0.299	0.349	0.629	0.565	0.486	0.246	0.967	0.483	0.477	0.465	0.745	0.608
C_6H_6	0.000	0.000	0.000	0.000	0.000	0.005	0.000	0.000	0.000	0.005	0.000	0.000	0.005

Name	V0493B	V0493C	V0493D	V0493E	V0493F	V0493G	V0493H	V0493I	V0493J	V0495A	V0495B	V0495C	V0497A
Deg	333	335	339	341	346	347	351	352	355	181	182	198	258
CH_4	0.000	0.000	0.022	0.000	0.082	0.021	0.053	0.025	0.017	0.000	0.000	0.000	0.000
HF	0.000	0.000	0.000	0.000	0.000	0.000	0.000	0.000	0.000	0.000	0.000	0.000	0.000
N_2	0.091	0.028	0.323	0.133	0.284	0.233	0.234	0.218	0.133	0.000	0.000	0.000	0.000
C_2H_6	0.000	0.017	0.000	0.000	0.000	0.209	0.000	0.000	0.000	0.000	0.000	0.000	0.000
C_3H_8	0.066	0.052	0.112	0.068	0.127	0.089	0.169	0.132	0.167	0.000	0.000	0.000	0.012
H_2S	0.010	0.018	0.026	0.021	0.015	0.027	0.028	0.025	0.037	0.000	0.000	0.000	0.000
HCl	0.000	0.000	0.000	0.000	0.000	0.000	0.000	0.000	0.000	0.000	0.000	0.000	0.000
H_2O	99.283	99.387	98.574	98.768	97.739	97.052	98.113	98.556	98.627	99.846	99.707	99.941	95.904
Ar	0.017	0.010	0.016	0.010	0.025	0.048	0.030	0.055	0.027	0.012	0.009	0.000	0.000
C_5H_{12}	0.020	0.025	0.039	0.030	0.000	0.051	0.038	0.074	0.058	0.000	0.000	0.000	0.018
C_4H_{10}	0.000	0.000	0.000	0.000	0.241	0.000	0.000	0.000	0.000	0.000	0.000	0.000	0.000
SO_2	0.049	0.032	0.152	0.119	0.508	0.372	0.306	0.152	0.223	0.000	0.000	0.000	0.000
CO_2	0.463	0.431	0.731	0.846	0.959	1.888	1.017	0.763	0.705	0.120	0.284	0.059	4.066
C_6H_6	0.000	0.000	0.000	0.005	0.021	0.010	0.010	0.000	0.005	0.000	0.000	0.000	0.000

Name	V0497B	V0497C	V0497D	V0497E	V0498A	V0498B	V0498C	V0498D	V0498E	V0498F	V0498G	V0498H	V0498I
Deg	265	271	274	275	296	296	300	301	310	311	313	313	315
CH_4	0.000	0.000	0.000	0.000	0.005	0.007	0.054	0.024	0.028	0.028	0.007	0.000	0.019
HF	0.000	0.000	0.000	0.000	0.000	0.000	0.000	0.000	0.000	0.000	0.000	0.000	0.000
N_2	0.000	0.000	0.000	0.000	0.020	0.050	0.000	0.000	0.039	0.000	0.008	0.068	0.027
C_2H_6	0.000	0.000	0.000	0.000	0.000	0.000	0.000	0.000	0.000	0.000	0.000	0.000	0.000
C_3H_8	0.000	0.000	0.000	0.000	0.061	0.155	0.074	0.045	0.112	0.158	0.059	0.068	0.234
H_2S	0.000	0.000	0.000	0.000	0.009	0.010	0.000	0.002	0.010	0.000	0.000	0.010	0.018
HCl	0.000	0.000	0.000	0.000	0.000	0.000	0.000	0.000	0.000	0.000	0.000	0.000	0.000
H_2O	93.300	97.334	97.335	98.430	99.275	99.032	99.056	99.660	99.210	98.828	99.629	99.630	99.315
Ar	0.003	0.002	0.002	0.009	0.002	0.003	0.008	0.001	0.010	0.009	0.004	0.003	0.002
C_5H_{12}	0.000	0.000	0.000	0.000	0.000	0.059	0.000	0.000	0.000	0.000	0.000	0.021	0.000
C_4H_{10}	0.000	0.000	0.000	0.000	0.186	0.000	0.226	0.076	0.155	0.191	0.094	0.000	0.040
SO_2	0.000	0.000	0.000	0.000	0.015	0.015	0.015	0.003	0.015	0.015	0.000	0.000	0.032
CO_2	6.697	2.664	2.664	1.561	0.427	0.669	0.568	0.190	0.420	0.772	0.199	0.199	0.309
C_6H_6	0.000	0.000	0.000	0.000	0.000	0.000	0.000	0.000	0.000	0.000	0.000	0.000	0.000

Name	V0499A	V0499B	V0499C	V0500A	V0500B	V0502A	V0502B	V0503A	V0503B	V0503C	V0504A	V0504B	V0506A
Deg	337	338	347	373	382	220	238	266	268	272	311	314	374
CH_4	0.000	0.000	0.029	0.010	0.089	0.466	0.249	0.385	0.300	0.644	0.400	0.663	0.133
HF	0.000	0.000	0.000	0.028	0.010	0.010	0.000	0.013	0.000	0.083	0.000	0.005	0.000
N_2	0.042	0.091	0.097	0.000	0.141	0.000	0.325	0.178	0.207	0.000	0.210	0.300	0.546
C_2H_6	0.000	0.000	0.000	0.267	0.423	0.000	0.000	0.000	0.839	0.000	0.000	0.000	0.000
C_3H_8	0.066	0.084	0.088	0.004	0.148	1.210	1.108	1.189	1.041	0.000	1.842	4.456	0.485
H_2S	0.047	0.028	0.018	0.068	0.079	0.815	2.477	0.242	0.540	0.466	0.239	0.180	0.252
HCl	0.000	0.000	0.000	0.000	0.000	0.000	0.000	0.000	0.000	0.000	0.000	0.000	0.000
H_2O	99.453	99.169	99.141	98.599	97.490	95.107	89.370	95.141	93.000	93.821	93.770	90.614	96.939
Ar	0.009	0.014	0.008	0.046	0.099	0.093	0.295	0.160	0.298	0.327	0.208	0.262	0.121
C_5H_{12}	0.019	0.019	0.000	0.049	0.101	0.079	0.527	0.110	0.307	0.575	0.000	0.000	0.135
C_4H_{10}	0.000	0.000	0.082	0.000	0.000	0.000	0.000	0.000	0.000	0.000	0.894	1.455	0.290
SO_2	0.032	0.032	0.032	0.049	0.131	0.028	0.374	0.095	0.480	0.305	0.079	0.155	0.235
CO_2	0.331	0.558	0.495	0.870	1.242	0.350	5.169	2.467	2.879	3.665	2.268	1.820	0.783
C_6H_6	0.000	0.000	0.010	0.010	0.048	0.094	0.104	0.020	0.109	0.115	0.090	0.091	0.082

Name	V0507A	V0507B	V0509A	V0509B	V0509C	V0509D	V0509E	V0510A	V0510B	V0510C	V0510D	V0511A	V0511B
Deg	182	197	263	270	271	273	278	307	310	310	315	338	339
CH_4	0.000	0.005	0.019	0.038	0.036	0.000	0.025	0.000	0.012	0.020	0.010	0.031	0.057
HF	0.000	0.017	0.000	0.000	0.000	0.013	0.000	0.004	0.022	0.000	0.000	0.000	0.000
N_2	0.057	0.284	0.107	0.222	0.000	0.077	0.046	0.046	0.000	0.033	0.282	0.063	0.000
C_2H_6	0.072	0.000	0.000	0.000	0.000	0.037	0.000	0.000	0.000	0.000	0.000	0.000	0.000
C_3H_8	0.000	0.132	0.090	0.187	0.144	0.062	0.133	0.237	0.110	0.105	0.101	0.117	0.110
H_2S	0.008	0.009	0.038	0.017	0.018	0.000	0.018	0.018	0.009	0.008	0.010	0.018	0.018
HCl	0.027	0.047	0.056	0.063	0.000	0.040	0.029	0.021	0.051	0.000	0.000	0.000	0.035
H_2O	99.404	99.088	99.133	98.914	99.025	99.317	99.085	98.605	99.258	99.471	98.851	99.247	99.141
Ar	0.002	0.023	0.010	0.022	0.010	0.024	0.008	0.010	0.010	0.009	0.009	0.009	0.008
C_5H_{12}	0.000	0.000	0.043	0.041	0.044	0.027	0.035	0.000	0.063	0.043	0.000	0.000	0.030
C_4H_{10}	0.045	0.026	0.000	0.000	0.000	0.000	0.000	0.392	0.000	0.000	0.135	0.148	0.000
SO_2	0.032	0.066	0.015	0.049	0.032	0.032	0.015	0.032	0.032	0.015	0.015	0.015	0.015
CO_2	0.348	0.299	0.487	0.441	0.686	0.366	0.602	0.626	0.428	0.292	0.588	0.348	0.582
C_6H_6	0.005	0.005	0.005	0.005	0.005	0.005	0.005	0.010	0.005	0.005	0.000	0.005	0.005

Name	V0511C	V0511D	V0511E	V0511F	V0511G	V0511H	V0511I	V0511J	V0512A	V0512B	V0512C
Deg	341	343	345	345	348	350	353	355	377	383	385
CH_4	0.000	0.009	0.000	0.042	0.059	0.000	0.037	0.000	0.038	0.000	0.196
HF	0.000	0.000	0.013	0.000	0.000	0.000	0.010	0.000	0.000	0.000	0.012
N_2	0.072	0.210	0.132	0.061	0.025	0.105	0.151	0.077	0.053	0.088	0.725
C_2H_6	0.000	0.000	0.000	0.000	0.000	0.000	0.053	0.000	0.148	0.357	0.309
C_3H_8	0.108	0.082	0.157	0.096	0.123	0.071	0.031	0.091	0.032	0.007	0.003
H_2S	0.018	0.030	0.010	0.022	0.027	0.018	0.322	0.018	0.039	0.025	0.055
HCl	0.000	0.000	0.000	0.000	0.000	0.000	0.000	0.000	0.000	0.000	0.000
H_2O	99.376	99.165	99.139	99.131	98.977	99.387	98.321	99.317	98.776	98.370	97.655
Ar	0.002	0.009	0.002	0.015	0.007	0.002	0.023	0.009	0.023	0.051	0.116
C_5H_{12}	0.027	0.000	0.000	0.000	0.000	0.000	0.000	0.017	0.030	0.049	0.085
C_4H_{10}	0.000	0.134	0.136	0.193	0.258	0.092	0.220	0.000	0.000	0.000	0.000
SO_2	0.015	0.015	0.032	0.032	0.015	0.032	0.048	0.015	0.032	0.083	0.065
CO_2	0.378	0.342	0.373	0.396	0.494	0.293	0.779	0.453	0.819	0.953	0.780
C_6H_6	0.005	0.005	0.005	0.010	0.016	0.000	0.005	0.005	0.010	0.016	0.000

APPENDIX 3: GAS CHEMISTRY OF NEA FLUIDS

Sample	V0224A	V0224B	V0224C	V0224D	V0228A	V0228B	V0228C	V0386A	V0386B	V0386C	V0387A	V0387B	V0387
Deg.C	242	270	334	396	289	351	372	309	317	319	361	368	374
CH_4	0.126	0.234	0.167	0.350	0.455	0.000	0.000	0.055	0.002	0.022	0.000	0.048	0.009
HF	0.000	0.000	0.000	0.000	0.000	0.000	0.000	0.000	0.000	0.003	0.007	0.016	0.009
N_2	0.000	0.000	0.000	0.000	0.000	0.000	0.000	0.129	0.089	0.015	0.025	0.089	0.059
C_2H_6	0.000	0.000	0.000	0.000	0.000	0.000	0.000	0.000	0.000	0.000	0.000	0.000	0.000
C_3H_8	0.418	0.709	0.309	0.000	1.405	0.000	0.000	0.000	0.000	0.000	0.000	0.000	0.000
H_2S	0.039	0.091	0.057	0.000	0.170	0.000	0.000	0.051	0.047	0.021	0.084	0.159	0.059
HCl	0.000	0.000	0.000	0.000	0.000	0.000	0.000	0.000	0.000	0.000	0.000	0.000	0.000
H_2O	94.856	94.517	95.302	70.462	96.351	90.307	87.955	99.342	99.452	99.695	99.608	98.671	99.085
Ar	0.019	0.039	0.026	0.034	0.088	0.018	0.012	0.024	0.010	0.001	0.002	0.016	0.018
C_5H_{12}	0.112	0.181	0.119	0.120	0.222	0.000	0.000	0.000	0.000	0.000	0.000	0.000	0.000
C_4H_{10}	0.000	0.000	0.000	0.000	0.000	0.000	0.000	0.000	0.000	0.000	0.000	0.000	0.000
SO_2	0.068	0.144	0.097	0.000	0.301	0.000	0.000	0.067	0.032	0.011	0.032	0.134	0.116
CO_2	4.361	4.082	3.919	29.005	0.993	9.675	12.034	0.333	0.367	0.232	0.242	0.867	0.645
C_6H_6	0.000	0.003	0.004	0.028	0.015	0.000	0.000	0.000	0.000	0.000	0.000	0.000	0.000

Sample	V0388A	V0388B	V0388C	V0388D	V0440A	V0440B	V0441A	V0441B	V0441C	V0441D	V0441E	V0442A	V0442B
Deg.C	395	405	408	412	275	287	325	325	333	334	341	363	368
CH_4	0.027	0.291	0.077	0.373	0.173	0.387	0.175	0.047	0.095	0.062	0.005	0.017	0.112
HF	0.000	0.000	0.000	0.054	0.000	0.013	0.024	0.000	0.000	0.000	0.000	0.000	0.008
N_2	0.095	0.152	0.898	0.146	0.172	0.000	0.000	0.000	0.000	0.000	0.000	0.459	0.423
C_2H_6	0.000	0.000	0.000	0.000	0.000	0.000	0.000	0.000	0.000	0.000	0.000	0.000	0.214
C_3H_8	0.000	0.000	0.000	0.000	0.000	0.952	0.390	0.141	0.269	0.141	0.090	0.194	0.350
H_2S	0.105	0.218	0.239	0.576	0.000	0.203	0.098	0.038	0.082	0.066	0.047	0.251	0.407
HCl	0.000	0.000	0.000	0.000	0.000	0.121	0.042	0.000	0.044	0.030	0.000	0.058	0.078
H_2O	98.073	96.535	98.056	95.035	97.967	96.730	97.707	98.751	98.252	98.712	99.241	96.895	96.395
Ar	0.030	0.224	0.179	0.150	0.000	0.017	0.037	0.009	0.022	0.017	0.009	0.112	0.025
C_5H_{12}	0.000	0.000	0.000	0.000	0.000	0.211	0.000	0.000	0.000	0.000	0.033	0.000	0.076
C_4H_{10}	0.000	0.000	0.000	0.000	0.000	0.000	0.474	0.329	0.354	0.329	0.042	0.441	0.000
SO_2	0.151	0.450	0.201	0.103	0.000	0.165	0.031	0.015	0.015	0.015	0.015	0.082	0.131
CO_2	1.520	2.131	0.350	3.563	1.689	1.190	1.015	0.666	0.857	0.623	0.513	1.434	1.706
C_6H_6	0.000	0.000	0.000	0.000	0.000	0.010	0.005	0.005	0.010	0.005	0.005	0.059	0.075

Sample	V0442D	V0474A	V0474B	V0474C	V0475A	V0475B	V0475C	V0475D
Deg.C	384	289	300	302	323	334	338	340
CH_4	0.298	0.205	0.068	0.279	9.702	0.886	0.246	0.238
HF	0.080	0.000	0.000	0.024	9.569	0.048	0.000	0.000
N_2	0.000	0.000	0.146	0.715	7.238	2.661	0.370	0.000
C_2H_6	0.579	0.123	0.057	0.000	0.000	0.000	0.000	0.494
C_3H_8	0.119	0.079	0.241	0.417	0.000	0.000	0.547	0.000
H_2S	0.825	0.050	0.049	0.055	3.968	0.172	0.119	0.077
HCl	0.285	0.110	0.063	0.139	0.919	0.057	0.071	0.011
H_2O	95.034	98.250	98.591	95.395	48.270	90.892	96.371	96.900
Ar	0.043	0.077	0.017	0.141	0.931	0.162	0.204	0.048
C_5H_{12}	0.163	0.176	0.064	0.000	0.000	0.000	0.000	0.221
C_4H_{10}	0.000	0.000	0.243	1.250	0.000	2.197	1.514	0.000
SO_2	0.245	0.134	0.049	0.148	0.000	0.357	0.115	0.113
CO_2	2.229	0.796	0.395	1.389	9.974	2.117	0.341	1.855
C_6H_6	0.101	0.000	0.016	0.048	8.684	0.453	0.103	0.042

APPENDIX 4: GAS CHEMISTRY OF MAJOR MAIN AND LATE STAGE FLUIDS FROM STABLE ISOTOPE STUDIES

Name	V0400A	V0400A	V0401A	V0401B	V0402A	V0414A	V0415A	V0419A	V0420A	V0420B	V0420C	V0421A	V0421B
TEMP	267	701	317	332	365	365	402	290	317	318	329	362	368
CH_4	0.030	0.507	0.431	0.461	0.081	0.073	0.086	0.034	0.897	0.344	0.270	0.177	0.042
HF	0.000	0.016	0.047	0.000	0.000	0.000	0.000	0.000	0.000	0.000	0.000	0.000	0.000
N_2	0.005	0.245	3.488	0.526	0.004	0.000	0.000	0.022	0.000	0.000	1.632	0.140	0.009
C_2H_6	0.000	0.000	0.000	0.000	0.000	0.000	0.000	0.000	1.386	0.000	0.000	0.000	0.000
C_3H_8	0.098	1.706	0.000	0.000	0.292	0.000	0.000	0.242	2.596	0.502	0.000	0.000	0.315
H_2S	0.027	0.067	0.480	0.140	0.115	1.638	1.091	0.010	0.142	0.095	0.272	0.185	0.118
HCl	0.000	0.053	0.000	0.000	0.000	0.000	0.000	0.000	0.183	0.076	0.000	0.000	0.000
H_2O	99.659	95.296	91.075	97.734	98.270	81.878	94.365	98.967	91.139	96.249	95.569	96.380	98.379
Ar	0.002	0.061	0.220	0.038	0.031	0.062	0.018	0.009	0.170	0.036	0.167	0.114	0.035
C_5H_{12}	0.000	0.000	0.000	0.000	0.000	0.502	0.000	0.000	0.000	0.000	0.652	0.000	0.000
C_4H_{10}	0.071	0.959	0.000	0.000	0.347	0.000	0.000	0.220	1.876	1.314	0.000	0.568	0.215
SO_2	0.003	0.052	0.138	0.048	0.049	9.614	2.144	0.015	0.123	0.048	0.097	0.148	0.066
CO_2	0.106	1.033	4.112	1.048	0.801	6.210	2.270	0.476	1.448	1.320	1.315	2.255	0.810
C_6H_6	0.000	0.004	0.009	0.005	0.010	0.022	0.026	0.005	0.040	0.016	0.026	0.032	0.010

Name	V0421C	V0428A	V0428B	V0429A	V0434A	V0436A	V0436B	V0446B	V0447A	V0448A	V0448B	V0448C	V0448D
TEMP	381	358	374	400	341	417	425	250	276	316	318	322	336
CH_4	0.015	0.171	0.237	0.007	0.150	0.026	0.035	0.201	0.279	0.736	0.147	0.119	0.058
HF	0.000	0.000	0.000	0.000	0.000	0.000	0.000	0.000	0.000	0.000	0.000	0.000	0.000
N_2	0.015	0.515	0.000	0.000	0.000	0.000	0.000	0.000	0.000	0.497	0.000	0.000	0.000
C_2H_6	0.127	0.012	0.358	0.002	0.000	0.000	0.000	0.091	0.000	0.000	0.000	0.000	0.000
C_3H_8	0.063	0.031	0.712	0.024	0.090	0.006	0.000	0.681	0.000	1.603	0.344	0.163	0.143
H_2S	0.115	0.284	0.311	0.169	0.953	1.399	1.752	0.388	0.198	0.166	0.130	0.049	0.050
HCl	0.000	0.271	0.000	0.000	0.000	0.000	0.118	0.000	0.000	0.000	0.000	0.000	0.000
H_2O	98.650	96.306	97.227	99.624	95.567	96.104	94.063	95.360	91.678	92.994	96.745	98.866	98.790
Ar	0.043	0.054	0.164	0.003	0.044	0.026	0.031	0.094	0.058	0.146	0.012	0.022	0.016
C_5H_{12}	0.000	0.162	0.000	0.000	0.000	0.000	0.000	0.000	0.000	0.238	0.000	0.000	0.000
C_4H_{10}	0.266	1.054	0.235	0.032	0.211	0.171	0.239	0.972	2.080	0.408	0.951	0.257	0.356
SO_2	0.032	0.031	0.065	0.003	1.440	0.081	0.000	0.244	0.658	0.174	0.115	0.031	0.032
CO_2	0.664	1.065	0.682	0.134	1.524	2.160	3.737	1.964	5.034	2.997	1.531	0.488	0.545
C_6H_6	0.010	0.043	0.010	0.001	0.021	0.026	0.026	0.005	0.015	0.041	0.027	0.005	0.010

Name	V0449A	V0449B	V0449C	V0450A	V0450B	V0450C	V0452A	V0453A	V0453A	V0455A	V0455B	V0455C	V0455D
TEMP	366	371	382	407	411	415	182	240	243	325	327	328	332
CH_4	0.252	0.141	0.033	0.029	0.097	0.287	0.066	0.000	0.000	0.007	0.012	0.000	0.000
HF	0.000	0.000	0.000	0.000	0.000	0.000	0.000	0.003	0.007	0.001	0.010	0.004	0.000
N_2	0.000	0.100	0.000	0.000	0.016	0.000	0.052	0.042	0.010	0.000	0.000	0.000	0.000
C_2H_6	0.384	0.317	0.176	0.000	0.666	0.000	0.000	0.000	0.000	0.000	0.000	0.000	0.000
C_3H_8	0.736	0.000	0.001	0.668	0.021	0.437	0.216	0.061	0.103	0.081	0.105	0.074	0.075
H_2S	0.759	0.208	0.265	0.406	0.351	0.642	0.056	0.018	0.030	0.047	0.070	0.039	0.039
HCl	0.000	0.000	0.000	0.000	0.000	0.000	0.037	0.000	0.000	0.000	0.000	0.000	0.000
H_2O	90.099	97.230	97.611	94.902	96.588	95.609	98.666	99.428	99.100	99.224	99.015	99.309	99.312
Ar	0.244	0.090	0.087	0.171	0.212	0.104	0.037	0.003	0.017	0.010	0.010	0.003	0.003
C_5H_{12}	0.000	0.000	0.000	0.000	0.000	0.000	0.000	0.000	0.000	0.000	0.000	0.000	0.000
C_4H_{10}	3.549	0.596	0.602	0.467	0.937	1.206	0.000	0.097	0.115	0.129	0.195	0.126	0.117
SO_2	0.513	0.115	0.133	0.210	0.114	0.343	0.066	0.032	0.049	0.032	0.032	0.015	0.015
CO_2	3.338	1.182	1.061	2.933	0.874	1.190	0.794	0.317	0.564	0.464	0.547	0.425	0.434
C_6H_6	0.126	0.021	0.032	0.214	0.124	0.182	0.010	0.000	0.005	0.005	0.005	0.005	0.005

Name	V0455E	V0455F	V0455G	V0456A	V0456B	V0456C	V0456D	V0456E	V0456F	V0456H	V0456I	V0456J	V0456L
Deg	333	314	318	356	358	359	361	362	363	367	369	370	374
CH_4	0.007	0.026	0.000	0.000	0.064	0.000	0.012	0.000	0.046	0.000	0.033	0.022	0.000
HF	0.008	0.000	0.000	0.001	0.088	0.024	0.012	0.000	0.015	0.000	0.002	0.009	0.019
N_2	0.001	0.000	0.000	0.000	0.000	0.000	0.000	0.000	0.000	0.000	0.000	0.000	0.000
C_2H_6	0.000	0.000	0.000	0.000	0.199	0.054	0.000	0.000	0.000	0.197	0.042	0.059	0.049
C_3H_8	0.122	0.171	0.087	0.079	0.109	0.051	0.070	0.047	0.099	0.062	0.118	0.094	0.034
H_2S	0.054	0.066	0.039	0.030	0.130	0.042	0.062	0.027	0.057	0.049	0.050	0.047	0.047
HCl	0.000	0.000	0.000	0.000	0.000	0.000	0.000	0.000	0.000	0.000	0.000	0.000	0.000
H_2O	99.166	98.957	99.301	99.330	98.055	99.180	98.900	99.240	99.051	98.762	98.958	98.889	99.177
Ar	0.016	0.017	0.002	0.017	0.030	0.016	0.031	0.016	0.017	0.022	0.017	0.017	0.016
C_5H_{12}	0.000	0.000	0.000	0.000	0.000	0.000	0.000	0.000	0.000	0.000	0.000	0.000	0.000
C_4H_{10}	0.179	0.248	0.088	0.086	0.360	0.144	0.189	0.103	0.185	0.252	0.153	0.184	0.152
SO_2	0.015	0.014	0.015	0.015	0.082	0.049	0.118	0.032	0.049	0.014	0.066	0.032	0.032
CO_2	0.426	0.496	0.463	0.437	0.856	0.435	0.590	0.530	0.472	0.630	0.549	0.638	0.464
C_6H_6	0.005	0.005	0.005	0.005	0.027	0.005	0.016	0.005	0.010	0.010	0.010	0.010	0.010

Name	V0456M	V0456N	V0456O	V0457A	V0457B	V0457C	V0457D	V0457E	V0457F	V0457G	V0457H
Deg	375	377	378	401	403	406	407	409	413	413	415
CH_4	0.030	0.000	0.000	0.037	0.047	0.000	0.108	0.137	0.051	0.000	0.049
HF	0.007	0.000	0.000	0.005	0.002	0.050	0.000	0.001	0.000	0.000	0.000
N_2	0.000	0.000	0.000	0.000	0.000	0.000	0.000	0.000	0.000	0.000	0.000
C_2H_6	0.035	0.035	0.000	0.000	0.143	0.046	0.000	0.155	0.000	0.421	0.093
C_3H_8	0.113	0.045	0.046	0.301	0.000	0.129	0.226	0.145	0.173	0.015	0.082
H_2S	0.090	0.038	0.030	0.206	0.093	0.232	0.286	0.378	0.182	0.221	0.186
HCl	0.000	0.000	0.000	0.000	0.000	0.000	0.000	0.000	0.000	0.000	0.000
H_2O	98.827	99.319	99.233	98.133	98.404	97.820	97.714	97.370	98.469	98.266	98.576
Ar	0.038	0.017	0.000	0.044	0.038	0.010	0.009	0.083	0.022	0.107	0.031
C_5H_{12}	0.000	0.000	0.000	0.000	0.000	0.000	0.000	0.000	0.000	0.000	0.000
C_4H_{10}	0.073	0.100	0.109	0.248	0.275	0.288	0.290	0.270	0.315	0.209	0.288
SO_2	0.066	0.032	0.032	0.116	0.066	0.201	0.133	0.246	0.100	0.083	0.066
CO_2	0.701	0.403	0.530	0.883	0.911	1.174	1.217	1.142	0.671	0.657	0.613
C_6H_6	0.022	0.010	0.010	0.027	0.021	0.049	0.016	0.072	0.016	0.021	0.016

APPENDIX 5: GAS COMPOSITION OF CARBONATE FLUIDS

SAMPLE	V0582A	582B	583C	583D	583E	583F	583G	587A	587B	588A	588B	588C	589A
TEMP	283	284	310	311	318	324	325	224	234	264	277	279	308
CONTRAST	1.09710	1.1230	1.56580	1.09709	1.19157	1.48796	1.30403	1.49157	1.15203	.33058	2.48980	1.22767	2.3977
RESIDUALS	.0042	.0050	.0037	.0079	.0066	.0039	.0031	.0022	.0028	.0036	.0031	.0055	.0033
H_2O	87.392	91.069	93.761	90.883	91.779	95.115	94.396	96.458	96.858	96.575	98.055	95.372	98.287
CO_2	5.857	6.135	5.286	3.259	6.188	3.891	3.585	2.260	.592	.553	1.495	3.029	1.283
H_2S	.166	.053	.043	.248	.087	.043	.070	.305	.263	.156	.021	.111	.018
SO_2	.333	.186	.030	.158	.221	.047	.063	.065	.021	.00	.021	.197	.014
N_2	.114	.00	.00	.00	.722	.00	.00	.00	1.155	.083	.012	.193	.00
CH_4	1.644	.670	.248	1.039	.722	.155	.190	.262	.120	.158	.00	.198	.032
C_2H_6	1.574	.350	.026	2.422	.00	.00	.00	.492	.296	.022	.045	.00	.00
C_3H_8	2.396	.886	.209	.875	.175	.292	1.067	.052	.348	.289	.235	.762	.271
C_5H_{12}	.318	.487	.313	.942	.578	.386	.434	.070	.327	.127	.086	.027	.086
C_6H_6	.048	.069	.005	.00	.088	.045	.034	.016	.019	.001	.006	.037	.007
Ar	.157	.096	.079	.176	.163	.026	.159	.019	.00	.040	.024	.074	.00
HCl	.00	.00	.00	.00	.00	.00	.00	.00	.00	.00	.00	.00	.00
HF	.00	.00	.00	.00	.00	.00	.00	.00	.00	.00	.00	.00	.00
NH_3	.00	.00	.00	.00	.00	.00	.00	.00	.00	.00	.00	.00	.00

SAMPLE	V0589B	589C	589D	589E	589F	589G	589H	595A	595B	595C	596A	596B	596C
TEMP	314	315	321	323	325	327	327	314	318	326	362	366	366
CONTRAST	19.53580	9.08827	1.49403	4.53225	10.60874	.58685	1.78906	1.62253	1.10808	1.68975	1.23020	1.70543	1.45870
RESIDUALS	.0045	.0047	.0033	.0037	.0043	.0045	.0045	.0030	.0035	.0086	.0034	.0046	.0039
H_2O	98.897	98.957	97.613	98.028	99.071	97.569	98.147	95.114	91.460	76.753	92.615	94.432	94.176
CO_2	.888	.867	1.910	1.561	.835	.930	1.20	4.013	5.307	22.656	5.458	4.759	4.548
H_2S	.008	.003	.025	.008	.003	.010	.010	.024	.027	.023	.048	.040	.056
SO_2	.00	.002	.031	.014	.001	.014	.014	.014	.108	.051	.046	.030	.014
N_2	.00	.00	.00	.00	.00	.00	.00	.232	.210	.00	.073	.00	.00
CH_4	.013	.003	.109	.077	.003	.00	.073	.032	.387	.110	.260	.164	.163
C_2H_6	.00	.00	.00	.00	.013	.00	.00	.00	.00	.141	.976	.00	.339
C_3H_8	.128	.113	.127	.186	.00	.265	.443	.467	1.589	.00	.006	.041	.293
C3H6	.00	.00	.00	.00	.00	.00	.00	.00	.841	.00	.00	.326	.253
C_5H_{12}	.048	.042	.134	.102	.061	.145	.086	.062	.033	.214	.262	.126	.089
C_6H_6	.006	.003	.023	.003	.004	.012	.00	.003	.039	.009	.113	.044	.041
Ar	.013	.010	.027	.020	.010	.055	.027	.039	.00	.043	.150	.039	.030
HCl	.00	.00	.00	.00	.00	.00	.00	.00	.00	.00	.00	.00	.00
HF	.00	.00	.00	.00	.00	.00	.00	.00	.00	.00	.00	.00	.00

SAMPLE	V0629A	629B	629C	630A	630B	630C	637A	637B	637C	643A	643B	643C	643D
TEMP	230.	242.	243.	269.	282.	286.	329.	332.	347.	309.	317.	319.	328.
CONTRAST	1.31098	1.14403	1.44298	1.40045	1.17440	1.19078	1.33894	1.08536	1.05462	.72958	7.73772	3.69822	1.24992
RESIDUALS	0.0043	0.0031	0.0054	0.0085	0.0073	0.0123	0.0044	0.0076	0.0094	.0057	0.0055	0.0071	0.0078
H_2O	98.506	98.478	98.252	97.750	96.799	96.104	96.340	95.559	90.785	96.919	98.244	98.508	97.387
CO_2	1.479	1.474	1.732	2.234	3.171	3.875	3.131	3.718	6.790	3.025	1.698	1.462	1.905
H_2S	0.000	0.000	0.000	0.000	0.000	0.000	0.017	0.065	0.051	0.000	0.000	0.000	0.000
SO_2	0.000	0.000	0.000	0.000	0.000	0.000	0.098	0.082	0.288	0.000	0.000	0.000	0.000
N_2	0.000	0.000	0.000	0.000	0.000	0.000	0.000	0.000	0.153	0.000	0.000	0.000	0.000
CH_4	0.000	0.022	0.000	0.000	0.000	0.000	0.091	0.155	0.243	0.006	0.026	0.000	0.000
C_2H_6	0.000	0.000	0.000	0.000	0.000	0.000	0.000	0.000	1.116	0.000	0.000	0.000	0.000
C_3H_8	0.000	0.000	0.000	0.000	0.000	0.000	0.211	0.125	0.000	0.000	0.000	0.000	0.000
C_3H_6	0.013	0.020	0.013	0.000	0.000	0.021	0.000	0.000	0.000	0.000	0.000	0.000	0.000
C_5H_{12}	0.000	0.000	0.000	0.017	0.024	0.000	0.093	0.183	0.351	0.048	0.028	0.028	0.033
C_6H_6	0.000	0.000	0.000	0.000	0.000	0.000	0.010	0.027	0.041	0.000	0.001	0.000	0.000
Ar	0.003	0.006	0.003	0.000	0.006	0.000	0.010	0.087	0.181	0.003	0.003	0.002	0.008
HCl	0.000	0.000	0.000	0.000	0.000	0.000	0.000	0.000	0.000	0.000	0.000	0.000	0.000
HF	0.000	0.000	0.000	0.000	0.000	0.000	0.000	0.000	0.000	0.000	0.000	0.000	0.000
NH_3	0.000	0.000	0.000	0.000	0.000	0.000	0.000	0.000	0.000	0.000	0.000	0.000	0.000

SAMPLE	V0647A	648A	648B	648C	648D	648E	649A	649B	649C	649D	649E	649F	654A
TEMP	244.	280.	288.	288.	292.	293.	315.	323.	329.	333.	333.	336.	280.
CONTRAST	1.92615	1.50483	1.48379	1.33480	2.11190	1.57466	1.66062	4.22180	1.64603	1.53354	1.16556	1.27124	1.15330
RESIDUALS	0.0071	0.0064	0.0057	0.0073	0.0078	0.0075	0.0074	0.0088	0.0077	0.0072	0.0100	0.0100	0.0059
H_2O	98.071	98.669	96.726	97.975	97.291	98.389	96.281	96.016	94.384	94.527	92.717	88.920	95.994
CO_2	1.905	1.312	3.253	2.004	2.690	1.593	3.690	4.218	5.537	5.374	7.204	10.937	3.507
H_2S	0.000	0.000	0.000	0.000	0.000	0.000	0.000	0.000	0.000	0.000	0.000	0.000	0.021
SO_2	0.000	0.000	0.000	0.000	0.000	0.000	0.000	0.000	0.000	0.000	0.000	0.000	0.081
N_2	0.000	0.000	0.000	0.000	0.000	0.000	0.000	0.000	0.000	0.000	0.000	0.000	0.000
CH_4	0.000	0.000	0.000	0.000	0.000	0.000	0.000	0.000	0.000	0.000	0.000	0.000	0.049
C_2H_6	0.000	0.000	0.000	0.000	0.000	0.000	0.000	0.000	0.000	0.000	0.000	0.000	0.001
C_3H_8	0.006	0.000	0.000	0.000	0.000	0.000	0.000	0.000	0.000	0.000	0.000	0.000	0.130
C_5H_{12}	0.014	0.017	0.017	0.014	0.018	0.016	0.026	0.030	0.077	0.096	0.079	0.136	0.018
C_6H_6	0.000	0.000	0.000	0.000	0.000	0.000	0.000	0.000	0.000	0.000	0.000	0.000	0.043
Ar	0.004	0.002	0.003	0.006	0.002	0.002	0.003	0.004	0.002	0.003	0.000	0.007	0.026
HCl	0.000	0.000	0.000	0.000	0.000	0.000	0.000	0.000	0.000	0.000	0.000	0.000	0.000
HF	0.000	0.000	0.000	0.000	0.000	0.000	0.000	0.000	0.000	0.000	0.000	0.000	0.000
NH_3	0.000	0.000	0.000	0.000	0.000	0.000	0.000	0.000	0.000	0.000	0.000	0.000	0.000

SAMPLE	V0654B	654C	655A	655B	655C	655D	656A	656B	660A	660B	661A	661B	665A
TEMP	282.	285.	327.	332.	334.	337.	364.	372.	277	295	322	327	243
CONTRAST	1.17390	1.24297	1.11665	1.15395	1.50951	1.17452	1.11048	1.13734	1.12753	1.15552	1.89754	1.22275	1.20785
RESIDUALS	0.0038	0.0069	0.0044	0.0054	0.0051	0.0076	0.0035	0.0051	0.0041	0.0028	0.0070	0.0080	0.0030
H_2O	96.449	97.471	92.762	92.180	95.808	92.005	93.957	88.316	91.751	91.802	45.611	92.364	95.384
CO_2	3.234	2.356	6.349	7.571	4.051	7.814	5.531	11.317	8.043	7.909	12.016	7.035	2.305
H_2S	0.009	0.010	0.032	0.009	0.008	0.007	0.017	0.019	.00	.005	.004	.00	.095
SO2	0.081	0.049	0.078	0.045	0.031	0.029	0.079	0.013	.157	.218	.375	.564	.278
N_2	0.000	0.000	0.000	0.000	0.000	0.000	0.000	0.000	.00	.00	.00	.00	.624
CH_4	0.005	0.000	0.156	0.031	0.002	0.000	0.077	0.104	.003	.027	.00	.00	.347
C_2H_6	0.000	0.000	0.243	0.000	0.000	0.000	0.000	0.000	.00	.00	.00	.00	.00
C_3H_8	0.004	0.000	0.105	0.000	0.000	0.000	0.014	0.000	.00	.00	.00	.00	.686
C_3H_6	0.000	0.000	0.000	0.000	0.000	0.000	0.000	0.000	.00	.00	.00	.00	.00
C_5H_{12}	0.123	0.095	0.185	0.125	0.064	0.099	0.125	0.134	.030	.030	.040	.029	.221
C_6H_6	0.026	0.005	0.020	0.025	0.015	0.025	0.047	0.034	.004	.004	.005	.004	.010
Ar	0.029	0.015	0.069	0.014	0.022	0.020	0.028	0.063	.013	.004	.009	.002	.049
HCl	0.000	0.000	0.000	0.000	0.000	0.000	0.000	0.000	.00	.00	.00	.00	.00
HF	0.000	0.000	0.000	0.000	0.000	0.000	0.000	0.000	.00	.00	.174	.00	.00
NH_3	0.000	0.000	0.000	0.000	0.000	0.000	0.000	0.000	.00	.00	41.766	.00	.00

SAMPLE	V0665A	665B	666A	666B	666C	667A	667B	667C	668A	668B	668C	668D	668E
TEMP	243	253	294	294	298	326	328	330	370	371	373	377	379
CONTRAST	1.20785	1.51481	2.68881	2.68881	1.21921	1.19573	1.29373	1.20835	1.50835	2.95196	1.70629	1.27115	1.24392
RESIDUALS	.0030	.0035	.0042	.0042	.0053	.0049	.0038	.0049	.0039	.0050	.0054	.0056	.0054
H_2O	95.384	91.004	91.896	91.896	93.717	95.599	88.491	93.701	90.848	90.966	96.674	89.491	84.043
CO_2	2.305	8.086	7.784	7.784	4.689	1.882	9.412	3.650	8.649	8.601	2.995	9.726	15.257
H_2S	.095	.033	.008	.008	.074	.038	.069	.068	.093	.123	.008	.064	.040
SO2	.278	.124	.093	.093	.112	.264	.333	.338	.202	.188	.250	.495	.216
N_2	.624	.00	.00	.00	.324	.432	.00	.00	.00	.00	.00	.00	.00
CH_4	.347	.260	.073	.073	.210	.197	.441	.391	.019	.026	.00	.037	.116
C_2H_6	.00	.00	.00	.00	.00	.00	.00	.00	.00	.00	.00	.00	.00
C_3H_8	.686	.331	.00	.00	.506	1.141	1.130	1.687	.00	.00	.00	.00	.00
C_5H_{12}	.221	.105	.127	.127	.254	.276	.00	.00	.106	.066	.052	.120	.173
C_6H_6	.010	.015	.004	.004	.042	.064	.044	.015	.035	.009	.010	.030	.056
Ar	.049	.043	.014	.014	.073	.107	.080	.100	.048	.021	.010	.037	.099
HCl	.00	.00	.00	.00	.00	.00	.00	.00	.00	.00	.00	.00	.00
HF	.00	.00	.00	.00	.00	.00	.00	.00	.00	.00	.00	.00	.00
NH_3	.00	.00	.00	.00	.00	.00	.00	.00	.00	.00	.00	.00	.00

SAMPLE	V0669A	669B	669C	670A	670B	670C	671A	671B	671C	671D	672A	672B	672C
TEMP	227	241	244	270	272	289	312	314	324	327	357	359	363
CONTRAST	1.52150	1.16328	1.68910	1.65128	1.99875	2.00635	1.68009	1.58710	1.72715	6.62189	3.00011	1.26151	1.14869
RESIDUALS	.0021	.0020	.0037	.0045	.0035	.0038	.0063	.0041	.0029	.0050	.0039	.0051	.0016
H_2O	8.460	96.344	98.618	98.913	99.066	99.547	99.257	99.556	97.867	98.704	98.391	97.141	92.474
CO_2	.974	2.051	1.072	.925	.730	.338	.702	.258	1.867	1.187	1.279	1.891	5.228
H_2S	.010	.041	.034	.018	.010	.00	.00	.008	.010	.00	.009	.051	.145
SO_2	.048	.146	.049	.032	.032	.015	.00	.015	.031	.015	.066	.201	.156
N_2	.00	.00	.00	.00	.00	.015	.00	.085	.00	.00	.00	.00	.00
CH_4	.111	.230	.046	.011	.00	.00	.00	.00	.080	.00	.012	.187	.265
C_2H_6	.169	.00	.00	.00	.064	.023	.00	.034	.00	.00	.001	.00	.257
C_3H_8	.167	.00	.115	.055	.075	.041	.022	.018	.091	.063	.168	.241	.856
C_5H_{12}	.027	.115	.058	.032	.021	.019	.015	.023	.050	.030	.059	.197	.420
C_6H_6	.016	.031	.005	.005	.00	.00	.00	.00	.00	.00	.00	.00	.00
Ar	.018	.067	.003	.009	.003	.003	.004	.003	.004	.002	.016	.047	.200
HCl	.00	.00	.00	.00	.00	.00	.00	.00	.00	.00	.00	.00	.00
HF	.00	.00	.00	.00	.00	.00	.00	.00	.00	.00	.00	.044	.00
NH_3	.00	.00	.00	.00	.00	.00	.00	.00	.00	.00	.00	.00	.00

SAMPLE	V0672D	672E	672F	672G	672H	672I	672J	672L	672M	679A	679B	686A	686B
TEMP	363	364	366	366	367	368	370	374	377	250.	244.	275	282
CONTRAST	1.12382	1.54635	1.34947	2.02054	1.33967	1.93075	1.34117	1.36025	1.11281	1.33093	1.12690	1.24411	1.18518
RESIDUALS	.0069	.0048	.0016	.0032	.0038	.0037	.0037	.0040	.0045	0.0072	0.0046	.0040	.0020
H_2O	94.725	97.157	96.495	97.072	97.488	97.620	96.948	96.532	90.921	98.100	97.305	94.598	94.631
CO_2	2.669	2.126	2.789	2.279	1.159	1.805	2.091	2.00	4.039	1.867	2.628	4.103	4.315
H_2S	.152	.026	.064	.021	.042	.017	.040	.065	.226	0.008	0.000	.041	.039
SO_2	.154	.031	.114	.082	.082	.116	.166	.065	.536	0.000	0.014	.063	.128
N_2	.00	.00	.00	.054	.00	.00	.00	.00	.00	0.000	0.018	.00	.003
CH_4	.739	.051	.194	.056	.117	.027	.154	.262	1.132	0.000	0.000	.117	.00
C_2H_6	.00	.00	.00	.164	.408	.085	.00	.478	.00	0.000	0.000	.545	.384
C_3H_8	1.205	.404	.096	.111	.394	.209	.335	.280	2.723	0.008	0.013	.212	.221
C_5H_{12}	.188	.140	.209	.115	.157	.063	.170	.150	.105	0.014	0.014	.197	.221
C_6H_6	.00	.010	.015	.021	.032	.027	.049	.054	.128	0.000	0.005	.010	.005
Ar	.155	.044	.060	.025	.121	.031	.048	.115	.190	0.003	0.002	.114	.138
HCl	.00	.00	.00	.00	.00	.00	.00	.00	.00	0.000	0.000	.00	.00
HF	.00	.00	.00	.00	.00	.00	.00	.00	.00	0.000	0.000	.00	.00
NH_3	.00	.00	.00	.00	.00	.00	.00	.00	.00	0.000	0.000	.00	.00

SAMPLE	V0686C	686D	686E	687A	687B	687C	687D	687E	687F	687G	687H	687I	687J
TEMP	284	288	288	320	322	323	325	325	325	326	328	331	333
CONTRAST	1.90569	1.24317	1.20336	1.10957	1.29809	1.16027	1.26814	1.48197	1.10260	1.16838	1.23806	3.03651	1.17175
RESIDUALS	.0032	.0027	.0040	.0023	.0038	.0024	.0028	.0039	.0035	.0017	.0024	.0040	.0053
H_2O	97.104	96.685	96.894	90.834	94.151	92.723	93.804	95.268	1.170	93.891	93.626	97.238	97.999
CO_2	2.609	2.526	1.964	7.065	4.969	5.948	5.328	4.211	5.429	4.471	5.482	2.478	1.390
H_2S	.018	.035	.040	.089	.032	.055	.019	.025	.054	.088	.033	.010	.042
SO_2	.048	.014	.098	.577	.014	.237	.175	.097	.203	.159	.158	.031	.100
N_2	.00	.00	.00	.00	.00	.00	.00	.00	.00	.191	.00	.00	.00
CH_4	.027	.062	.074	.309	.275	.449	.090	.102	.773	.00	.306	.038	.047
C_2H_6	.00	.177	.118	.00	.00	.00	.00	.00	.00	.00	.00	.00	.00
C_3H_8	.075	.285	.447	.546	.172	.00	.257	.046	1.406	.722	.00	.063	.227
C_5H_{12}	.080	.147	.118	.288	.246	.358	.206	.153	.447	.00	.256	.097	.129
C_6H_6	.016	.021	.038	.076	.052	.134	.025	.026	.200	.057	.031	.021	.033
Ar	.024	.048	.327	.217	.089	.095	.097	.072	.318	.183	.107	.025	.034
HCl	.00	.00	.00	.00	.00	.00	.00	.00	.00	.00	.00	.00	.00
HF	.00	.00	.00	.00	.00	.00	.00	.00	.00	.00	.00	.00	.00
NH_3	.00	.00	.00	.00	.00	.00	.00	.00	.00	.00	.00	.00	.00

APPENDIX 6: GAS COMPOSITIONS OF QUARTZ FLUIDS FROM PMB-BY LOCALITY IN THE OH VEIN

SAMPLE	V0513A	V0513B	V0513C	V0514A	V0514B	V0514C	V0514D	V0514E	V0514F	V0514G	V0514H	V0515A	V0515B
TEMP	191	195	200	221	223	224	228	230	230	236	240	268	269
CONTRAST	1.03	1.16	1.14	1.29	1.22	1.21	1.70	1.36	1.29	1.16	1.32	1.72	8.92
RESIDUALS	.0026	.0029	.0026	.0021	.0025	.0045	.0015	.0020.	.0036	.0034	.0021	.0021	.0037
H_2O	97.034	96.019	93.798	15.580	94.616	97.569	97.215	97.524	97.366	96.612	96.751	98.792	99.598
CO_2	.906	1.072	1.391	54.853	3.640	.752	2.057	1.737	1.919	1.552	2.012	.871	.298
H_2S	.271	.092	.235	19.846	.728	.437	.224	.231	.302	.264	.176	.018	.004
SO_2	.165	.313	.301	.410	.352	.180	.081	.132	.048	.112	.114	.014	.008
N_2	.0	1.131	.467	1.373	.0	.162	.004	.0	.0	.462	.0	.0	.0
CH_4	.0	.472	.590	.846	.283	.256	.067	.146	.118	.109	.317	.046	.024
C_2H_6	.788	.0	1.934	1.373	.0	.0	.0	.0	.0	.148	.0	.0	.0
C_3H_8	.159	.499	.728	.159	.004	.509	.233	.040	.194	.332	.544	.210	.052
C_5H_{12}	.906	.045	.044	.577	.099	.044	.059	.116	.035	.233	.048	.027	.014
C_6H_6	.060	.048	.067	.055	.026	.037	.005	.016	.0	.037	.021	.005	.001
Ar	.153	.311	.279	.323	.143	.055	.044	.057	.018	.140	.017	.0	.0
HCl	.0	.0	.165	.437	.136	.0	.0	.0	.0	.0	.0	.0	.0
HF	.0	.0	.0	.0	.0	.0	.0	.0	.0	.0	.0	.0	.0
NH_3	.0	.0	.0	.0	.0	.0	.0	.0	.0	.0	.0	.0	.0

SAMPLE	V0515C	V0515D	V0515E	V0515F	V0516A	V0516B	V0516C	V0516D	V0516E	V0517A	V0517B	V0517C	V0517D
TEMP	271	271	275	277	303	305	313	314	317	339	344	350	354
CONTRAST	2.61	1.26	3.99	2.21	3.00	2.12	1.30	1.44	1.95	1.33	1.64	3.54	1.56
RESIDUALS	.0016	.0066	.0064	.0042	.0038	.0036	.0050	.0041	.0036	.0037	.0046	.0051	.0039
H_2O	99.369	99.676	99.499	99.433	99.520	99.563	98.936	99.580	99.570	99.457	99.405	99.555	99.184
CO_2	.502	.240	.379	.345	.302	.260	.871	.222	.231	.268	.291	.217	.472
H_2S	.008	.010	.008	.010	.002	.002	.010	.004	.002	.008	.008	.010	.010
SO_2	.015	.015	.015	.015	.008	.008	.015	.003	.003	.015	.015	.015	.015
N_2	.0	.0	.0	.052	.0	.0	.0	.0	.017	.037	.0	.030	.076
CH_4	.029	.0	.0	.0	.038	.038	.014	.040	.040	.028	.018	.0	.024
C_2H_6	.0	.0	.0	.0	.0	.0	.0	.0	.0	.0	.0	.0	.0
C_3H_8	.052	.047	.0761	.106	.101	.102	.072	.116	.102	.134	.202	.129	.118
C_5H_{12}	.020	.011	.022	.030	.022	.020	.059	.024	.026	.032	.040	.030	.072
C_6H_6	.0	.0	.0	.0	.001	.001	.005	.003	.001	.005	.005	.005	.005
Ar	.005	.002	.002	.009	.006	.006	.017	.008	.008	.017	.016	.010	.024
HCl	.0	.0	.0	.0	.0	.0	.0	.0	.0	.0	.0	.0	.0
HF	.0	.0	.0	.0	.0	.0	.0	.0	.0	.0	.0	.0	.0
NH_3	.0	.0	.0	.0	.0	.0	.0	.0	.0	.0	.0	.0	.0

SAMPLE	V0517F	V0518A	V0518B	V0518C	V0518D	V0518E	V0518F	V0519E	V0519F	V0519G	V0519A	V0519D	V0519B
TEMP	355	384	389	381	382	384	390	414	414	415	418	419	422
CONTRAST	5.42	1.02	1.02	1.18	1.55	1.09	1.22	1.14	1.10	1.18	1.09	1.09	1.01
RESIDUALS	.0043	.0189	.0042	.0052	.0037	.0059	.0055	.0039	.0068	.0049	.0095	.0074	.0155
H_2O	99.483	92.874	76.605	98.546	98.939	97.925	98.672	97.734	96.589	97.469	67.653	86.160	59.769
CO_2	.284	2.158	9.206	1.005	.589	1.003	.574	.443	1.509	1.069	15.007	12.295	10.890
H_2S	.004	.291	.051	.055	.018	.049	.047	.085	.131	.037	.140	.215	.556
SO_2	.008	1.319	3.940	.049	.049	.126	.032	.116	.138	.048	16.107	.216	9.151
N_2	.029	1.290	1.176	.0	.108	.040	.201	.0	.0	.0	.0	.0	.0
CH_4	.044	.911	1.434	.022	.032	.226	.049	.073	.352	.271	.498	.605	5.586
C_2H_6	.0	.0	.0	.124	.066	.209	.0	1.302	.0	.728	.0	.0	10.445
C_3H_8	.102	.183	.0	.070	.097	.123	.295	.0	.818	.0	.0	.0	.0
C_5H_{12}	.028	.111	1.134	.061	.043	.181	.042	.060	.106	.081	.175	.227	.756
C_6H_6	.004	.098	.265	.033	.022	.074	.039	.049	.138	.038	.244	.075	.753
Ar	.013	.0	.296	.036	.036	.045	.050	.138	.226	.087	.175	.162	1.270
HCl	.0	.0	.292	.0	.0	.0	.0	.0	.132	.173	.0	.046	.826
HF	.0	.764	.0	.0	.0	.0	.0	.0	.0	.0	.0	.0	.0
NH_3	.0	.0	5.598	.0	.0	.0	.0	.0	.0	.0	.0	.0	.0

SAMPLE	V0519C	V0519H	V0519I
TEMP	427	423	433
CONTRAST	1.01	1.34	1.09
RESIDUALS	.0726	.0033	.0024
H_2O	13.020	98.341	94.092
CO_2	9.169	.760	3.588
H_2S	4.984	.070	.150
SO_2	28.442	.083	.238
N_2	.0	.0	.0
CH_4	7.966	.127	.226
C_2H_6	25.968	.097	.0
C_3H_8	.0	.261	1.077
C_5H_{12}	5.114	.090	.046
C_6H_6	2.944	.071	.105
Ar	2.026	.033	.309
HCl	.367	.067	.168
HF	.0	.0	.0
NH_3	.0	.0	.0